SIT-AFOSR-N-85.86.87-1

AFOSR-TR- 88-0902

Mega-Amp Opening Switch with Nested Electrodes/Pulsed Generator of Ion and Ion Cluster Beams

V. Nardi

July 30, 1987

Final Report
(and Annual Report
for the period
June 1, 1986 - June 30, 1987)

AFOSR 1984-1987

Grant No. AFOSR-84-0228

S INSTITUTE
TECHNOLOGY
STEVENS POINT
NEW JERSEY 07030

DISCLAIMER NOTICE

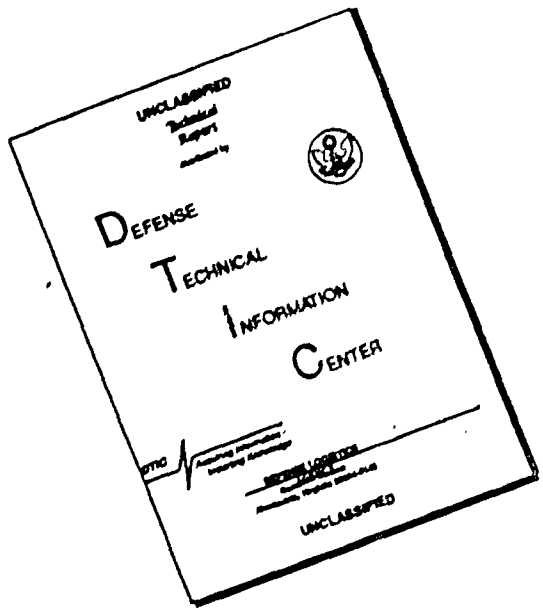

THIS DOCUMENT IS BEST QUALITY AVAILABLE. THE COPY FURNISHED TO DTIC CONTAINED A SIGNIFICANT NUMBER OF PAGES WHICH DO NOT REPRODUCE LEGIBLY.

Unclassified

SECURITY CLASSIFICATION OF THIS PAGE

REPORT DOCUMENTATION PAGE

1a. REPORT SECURITY CLASSIFICATION Unclassified	1b. RESTRICTIVE MARKINGS
2a. SECURITY CLASSIFICATION AUTHORITY	3. DISTRIBUTION/AVAILABILITY OF REPORT Approved for public release, distribution unlimited
2b. DECLASSIFICATION/DOWNGRADING SCHEDULE	
4. PERFORMING ORGANIZATION REPORT NUMBER(S) SIT-AFOSR-N-85.86.87-1	5. MONITORING ORGANIZATION REPORT NUMBER(S) AFOSR-TR- 88-0902
6a. NAME OF PERFORMING ORGANIZATION Stevens Institute of Technology 6b. OFFICE SYMBOL (If applicable)	7a. NAME OF MONITORING ORGANIZATION AFOSR
6c. ADDRESS (City, State and ZIP Code) Castle Point Hoboken, NY 07030	7b. ADDRESS (City, State and ZIP Code) Bldg 410 Bolling AFB DC 20332-6448
8a. NAME OF FUNDING/SPONSORING ORGANIZATION AFOSR 8b. OFFICE SYMBOL (If applicable) NP	9. PROCUREMENT INSTRUMENT IDENTIFICATION NUMBER AFOSR-84-0228
8c. ADDRESS (City, State and ZIP Code) Bldg 410 Bolling AFB DC 20332-6448	10. SOURCE OF FUNDING NOS. PROGRAM ELEMENT NO.: 61102F PROJECT NO.: 2201 TASK NO.: 07 WORK UNIT NO.:
11. TITLE (Include Security Classification) (U) Mega-Amp Opening Switch with Nested Electrodes/Pulsed Generator of Ion and Ion Cluster Beams	
12. PERSONAL AUTHOR(S) V. Nardi	
13a. TYPE OF REPORT Final 13b. TIME COVERED FROM Jun 1 86 TO Jun 30 87	14. DATE OF REPORT (Yr., Mo., Day) July 30, 1987 15. PAGE COUNT 38
16. SUPPLEMENTARY NOTATION	
17 COSATI CODES FIELD / GROUP / SUB. GR.	18. SUBJECT TERMS (Continue on reverse if necessary and identify by block number) Plasma Focus Voltage Neutron
19. ABSTRACT (Continue on reverse if necessary and identify by block number) See Other Side	
20. DISTRIBUTION/AVAILABILITY OF ABSTRACT UNCLASSIFIED/UNLIMITED ☒ SAME AS RPT. ☐ DTIC USERS ☐	21. ABSTRACT SECURITY CLASSIFICATION Unclassified
22a. NAME OF RESPONSIBLE INDIVIDUAL Lt Col Bruce L. Smith	22b. TELEPHONE NUMBER (Include Area Code) 202-767-4994 22c. OFFICE SYMBOL NP

DD FORM 1473, 83 APR EDITION OF 1 JAN 73 IS OBSOLETE.

SECURITY CLASSIFICATION OF THIS PAGE

The use of a plasma focus as an MA opening switch has been demonstrated by two modes of operation: (A) Single shot Mode; (B) Repetitive Mode with a repetition rate of 0.1-1 MHz. The peak current in (A) was ~ 0.6 MA (from a 8 kJ capacitor bank at 18 kV) and in (B) ~ 0.2 MA (from a 40 kJ pulse forming network at ~40 kV). A voltage multiplication by a factor $\gtrsim$ 7 was observed during the 0.1 μs opening stage in (A), and by a factor ~ 2.4 in (B). The use of field distortion elements (FDE, say) in the interelectrode gap indicates that the neutron yield (from D-D fusion reactions; deuterium filling of the discharge chamber) increased by a factor 10 as compared to the yield of the same system operating at the same energy level and under the same voltage and filling-pressure conditions but without field distortion elements. Misfirings of the plasma focus machine are also virtually eliminated by using an FDE at the coaxial electrode breech. In the course of our tests (based on about 10^4 shots and five plasma focus machines) we have also demonstrated that a sizable amount of nuclear reactions with high-Z nuclei (C,N) are induced by the MeV D^+ ions which are accelerated and trapped in the pinch when we enter in the filling gas D_2+1-15% of carbon (or nitrogen) atoms. The observed reaction yield for high-Z nuclei is increased by suitable FDE's and is about 3% of the D-D fusion reaction yield. The neutron yield Y_n provides for all shots (with or without FDE's) a good quantitative estimate of the performance of the plasma focus as an opening switch, i.e., Y_n is strongly correlated with the drop of the electrode current (I) during the "opening" stage.

Mega-Amp Opening Switch with Nested Electrodes/Pulsed Generator of Ion and Ion Cluster Beams

V. Nardi

Final Report

and

Report for the Period July 1, 1986 - June 30, 1987

Information and experimental data entered in this report
have been contributed by
V. Nardi, L. Bilbao, W. H. Bostick, J. Brzosko, M. Esper
C. M. Luo, C. Powell, D. Zeng

AFOSR 1984-1987

Grant No. AFOSR-84-0228

July 30, 1987

Summary

The use of a plasma focus as an MA opening switch has been demonstrated by two modes of operation: (A) Single shot Mode; (B) Repetitive Mode with a repetition rate of 0.1-1 MHz. The peak current in (A) was ~ 0.6 MA (from a 8 kJ capacitor bank at 18 kV) and in (B) ~ 0.2 MA (from a 40 kJ pulse forming network at ~40 kV). A voltage multiplication by a factor $\gtrsim$ 7 was observed during the 0.1 μs opening stage in (A), and by a factor ~ 2.4 in (B). The use of field distortion elements (FDE, say) in the interelectrode gap indicates that the neutron yield (from D-D fusion reactions; deuterium filling of the discharge chamber) increased by a factor 10 as compared to the yield of the same system operating at the same energy level and under the same voltage and filling-pressure conditions but without field distortion elements. Misfirings of the plasma focus machine are also virtually eliminated by using an FDE at the coaxial electrode breech. In the course of our tests (based on about 10^4 shots and five plasma focus machines) we have also demonstrated that a sizable amount of nuclear reactions with high-Z nuclei (C,N) are induced by the MeV D^+ ions which are accelerated and trapped in the pinch when we enter in the filling gas D_2 + 1-15% of carbon (or nitrogen) atoms. The observed reaction yield for high-Z nuclei is increased by suitable FDE's and is about 3% of the D-D fusion reaction yield. The neutron yield Y_n provides for all shots (with or without FDE's) a good quantitative estimate of the performance of the plasma focus as an opening switch, i.e., Y_n is strongly correlated with the drop of the electrode current (I) during the "opening" stage.

List of Publications 1987

1. V. Nardi, C. M. Luo, C. Powell, J. Brzosko: Confinement of MeV Ions in a Dense Pinch. Proc. 13th Eur. Conf. on Controlled Fusion and Plasma Heating (Schliersee, FRG, 14-18 April 1986), Editors: G. Brifford, M. Kaufmann, Publisher: E. Phys. Soc., Vol. 10C, Part 1, pp. 368-371(1987).

2. V. Nardi, C. M. Luo, C. Powell: Ion Clusters from Focused MA Discharges, Proc. 6th Int. Conf. on High-Power Particle Beams (Beams '86 Kobe, Japan, June 9-12, 1986), C. Yamamaka, Edit. (ILE, Osaka University, 1987), p. 447-450.

3. V. Nardi: Production of Ion Clusters in MG Fields, Contrib. to Megagauss Magnetic Field Generation, Edit. C. M. Fowler (Los Alamos N.L.) PLENUM, New York, 1987, p. 269-277.

4. J. Brzosko, M. Esper, V. Nardi, C. Powell, D. Zeng (in cooperation with the Univ. of Ferrara): Improved Self-Field Confinement of Hot Plasma with Fusion Reactions, Proc. 14th Eur. Conf. on Controlled Fusion and Plasma Physics, (Madrid, 1987), F. Engelmann & Alvarex Rivas Edit's., Vol. 11D, (part 2) p. 548.

5. V. Nardi, F. Gratton, G. Gnavi: A Hamiltonian Method to Derive Three Dimensional Oscillatory Vlasov Structures with a Magnetic Field, Proc. 14th Eur. Conf. on Controlled Fusion and Plasma Physics, (Madrid, 1987), F. Engelmann, J. L. Alvarez Rivas, Vol. 11D, (part 3) p. 1127.

6. V. Nardi, F. Gratton, G. Gnavi: Exact Solutions for Perturbations of Vlasov-Poisson Structures, Phys. L., 121A, 427 (1987).

7. V. Nardi, J. Brzosko: The Advanced Plasma Focus as Neutron Source for Neutron Radiography, contrib. to the "Nuclear Resonance Radiography Workshop" June 1987, (Lynn edit., LANSCE, Los Alamos N. Lab).

8. V. Nardi, A. Bortolotti, J. S. Brzosko, M. Esper, C. M. Luo, F. Pedrielli, C. Powell: Stimulated Acceleration and Confinement of Deuterons in Focused Discharges (Part I), IEEE Transact. Plasma Sci., 16, 368 (1988).

9. V. Nardi, L. Bilbao, a. bortolotti, J. Brzosko, F. Mezzetti, C. Powell, D. Zeng: Stimulated Acceleration and Confinement of Deuterons in Focused Discharges (Part II), IEEE Transact. Plasma Sci. 16, 374 (1988).

10. V. Nardi, D. Zeng, M. Esper, C. Powell: Repetitive Mode of Operation of a Plasma Focus as MA-Opening Switch, prepared for publication.

List of Completed Experiments and Results

During the period of three years of the research contract we have (a) detected and clarified basic physics processes occurring in the plasma pinch of focused discharges, (b) improved the performance of focused-discharge systems as MA opening switches, and (c) brought close to completion the construction of an upgraded plasma focus machine of 200 kJ at 60 kV. We list under (a):

1. The production in deuterium and hydrogen discharges of heavy ion clusters with a mass/charge ratio from $m/z \sim 1$ to $m/z \gg 10^6$ (in atomic units) with MeV ions. [Ref. 1,2].

2. Determination of time and space structure of the source and of source-brightness characteristics. [Ref. 3 and ref. quoted therein].

3. Focalization of kA ion-beams in pulsed magnetic lenses and ion-beam charge neutralization with relativistic electron beams for low-energy plasma-focus machines (6-15 kJ). [Ref. 4 and Appendix 1 of this Report].

4. Determination of the typical linear dimensions (λ) of the extremely-localized regions of space within the source where ion acceleration starts and is completed ($\lambda \sim 100$ μm) with an ion-energy gain greater by a factor 500 than the energy corresponding to the externally applied voltage. [1,2,5 and ref. quoted therein].

5. Production of nuclear reactions with high-z atoms (B,C,N,O) inside the plasma source of the beam, where the self-magnetic field of the source is trapping the bulk of the accelerated D^+ ions. The produced amount of short-life isotopes from the reactions of high-z nuclei is a few percent of the amount of D-D fusion reactions. [4,6 and Appendix I of this Report].

6. Determination of the D^+ ion-energy spectrum as a function of time with a compact Thomson spectrometer (time resolution $\simeq$ 1 nanosec; a sinusoidal or, in a different mode of operation, a ramped electric field has been used with the time-dependent component $\tilde{E}(t>)$ of the same magnitude of the constant component $\bar{E}_o \sim 1$ kV/cm of the field). The low-energy D^+-ions ($\gtrsim$ 0.1 MeV) are ejected from the plasma source $\sim$ 100 nanosec earlier than the D^+ of energy $\gtrsim$ 1 MeV. The delay in the ion time of emission is tapering off with increasing values of the ion energy. [1,2,3,5,7].

The improvements listed under (b) have been obtained by using field-distortion elements (FDE) between the electrodes. The FDE's have the effect of:

1. Virtually eliminating the misfiring of the machine, so that the peak overvoltage during the "open" stage of the system reaches in the majority of the shots a value close or equal to seven times the initially applied voltage V_o on the electrodes (in a single shot mode of operation) and of increasing the neutron yield from D-D fusion reaction by a factor > 3-5 for the same voltage V_o and capacitor-bank energy W_o. [6,7,8].

2. Providing the possibility of a MHz-repetition-rate mode of operation of a plasma focus machine with a substantially reduced probability of bad

pinches (i.e. weak pinches without a corresponding x-ray pulse). We have tested this mode of operation by powering a small plasma focus machine (equivalent in size to a 1 kJ machine) with a pulse forming network with a constant ≅ 150 kA current pulse of duration 20 microsec, at a peak voltage $V_o \tilde{=}$ 40 kV (with a network loaded up to $W_o \sim$ 40 kJ). The maximum overvoltage in the MHz mode of operation is about 4 times the applied voltage V_o. [5]

3. Increasing the azimuthal uniformity and the sharp definition of the leading edge of the current sheath. With these improvements the imploding current sheath during a time interval of about 100 nanosec before the pinch formation is an aberration-free pulsed magnetic lens suitable for the focalization of very intense pulsed ion beams with any energy, from a few MeV to > GeV. [4]

4. Reducing the damage (boiling-off and heating) of the insulator at the breech of the coaxial-electrode system. This is a particularly important advantage in the repetitive mode of operation (~ 10 Hz or ~ 1 MHz) of the machine at high-power level. [5].

During the construction of the upgraded 200 kJ plasma focus machine (c) we have:

1. Manufactured and tested on thousands of shots five (30 nh) MA closing switches (one field-distortion switch is used for each of the five 40-kJ modules which power the machine) with acquisition of complete series of data about erosion (negligible) of the synthesized material (kulite) of the electrodes, and on the lifetime (>> 2000 shots) of the insulating-material components in the discharge-exposed volume inside each switch [5].

2. Tested new power-transmission lines (each formed of a pair of parallel plates > 2 yard long, suitable for the ~ 10 ns jitter of the switches) as on alternative to coaxial cables, with the purpose of reaching a higher charging voltage V_o of the capacitor bank, with acceptable breakdown limitations (on V_o) for switch-plate and for plate - plasma-focus-header connection. [5 and this Report].

3. Built and operated a 40 kJ (at $V_o \sim$ 40 kV) pulse-forming-network which generates a current pulse (20 μs^o long) of constant amplitude (150-200 kA) for switch testing, in parallel with the repetitive mode of operation (at a MHz repetition rate) of a plasma-focus opening switch. [5]

These results have been extensively reported in the following References (the appropriate Reference for each of the above items is indicated in square brackets).*

(*) To gain insight in the applications of plasma opening switches theoretical work on the mechanism of MeV ion acceleration in a "medium" type of accelerator (plasma waves with λ << 1 mm and plasma diodes, $\lambda \sim$ 1 mm) has progressed with the collaboration of visiting scientists. [9].

References

1. V. Nardi: Contrib. to Megagauss Technology and Pulsed Power Application (MG-IV), M. C. Fowler et al. Eds., Plenum, N.Y. (1987) p. 269-277.

2. V. Nardi, C. M. Luo, C. Powell: Proc. 6th Int. Conf. on High Power Particle Beams (Kobe, Japan 1986) p. 447-450.

3. V. Nardi, et al.: 13th Europ. Conf. on Controlled Fusion (Schliersee, FRG, 1986), Vol. 10C, part 1, p. 368-371.

4. J. S. Brzosko, V. Nardi, C. Powell, D. Zeng: (Acceptd for publication in the Proceed. of the 15th Europ. Conf. on Controlled Fusion; Dubrownik, May 1988, 4 pages).

5. V. Nardi: Annual Report for AFOSR (SIT-AFOSR-N-85.86.6) July 1, 1986, pp. 47.

6. V. Nardi, et al.: IEEE Trans. Plasma Sci., Vol. 16, 374 (1988), Part II.

7. V. Nardi: Annual Report for AFOSR (SIT-AFOSR-N-84.85.4) July 1, 1985, pp. 33.

8. V. Nardi, et al.: IEEE Trans. P{lasma Sci. Vol. 16, 368 (1988), Part I.

9. V. Nardi, F. Gratton, G. Gnavi: Phys. L. 121 A, 427 (1987), and Proc. 14th Europ. Conf. on Controlled Fusion (Madrid 1987), Vol. 11D (part 3) p. 1127. W.H. Bostick, V. Nardi: Proc. 19th Int. Cosmic Ray Conf. (LaJolla, CA, Aug. 1985), S. C. Jones, Edit. NASA Sci. & Tech. Br. (0G8.2-14) Vol. 3, 183 (1985).

Technical Details

Fig. 1–(a): Schematic view of pulse forming network/line with plasma focus (PF), anode (1), cathode (2), insulator (pyrex) sleeve (3), Rogowski coil (4) for measurements of the electrode current I and current variations $\dot{I}$ ($\equiv dI/dt$).

–(b): Equivalent circuit. The inductance L_i of the line between capacitors is determined from the construction geometry $L_i^{-1} = L_{ia}^{-1} + L_{ib}^{-1}$ ($L_{ia} = 4\pi x10^{-7} a\ell/c$, $L_{ib} = 4\pi x10^{-7} b\ell/c$ where c is the width of the hot plate, ℓ the distance between capacitors, a the distance of the hot plate HP from the lower grounded plate, b the distance of HP from the top grounded plate; see following photograph 1-C of pulse forming network). The trigger electrode of the main switch SW - before closing - is at the voltage $V_0/2$ (V_0 = hot plate voltage). A negative pulse - $V_0/2$ is used for shorting SW (H.V.D.C. is the high voltage DC line for charging the capacitors).

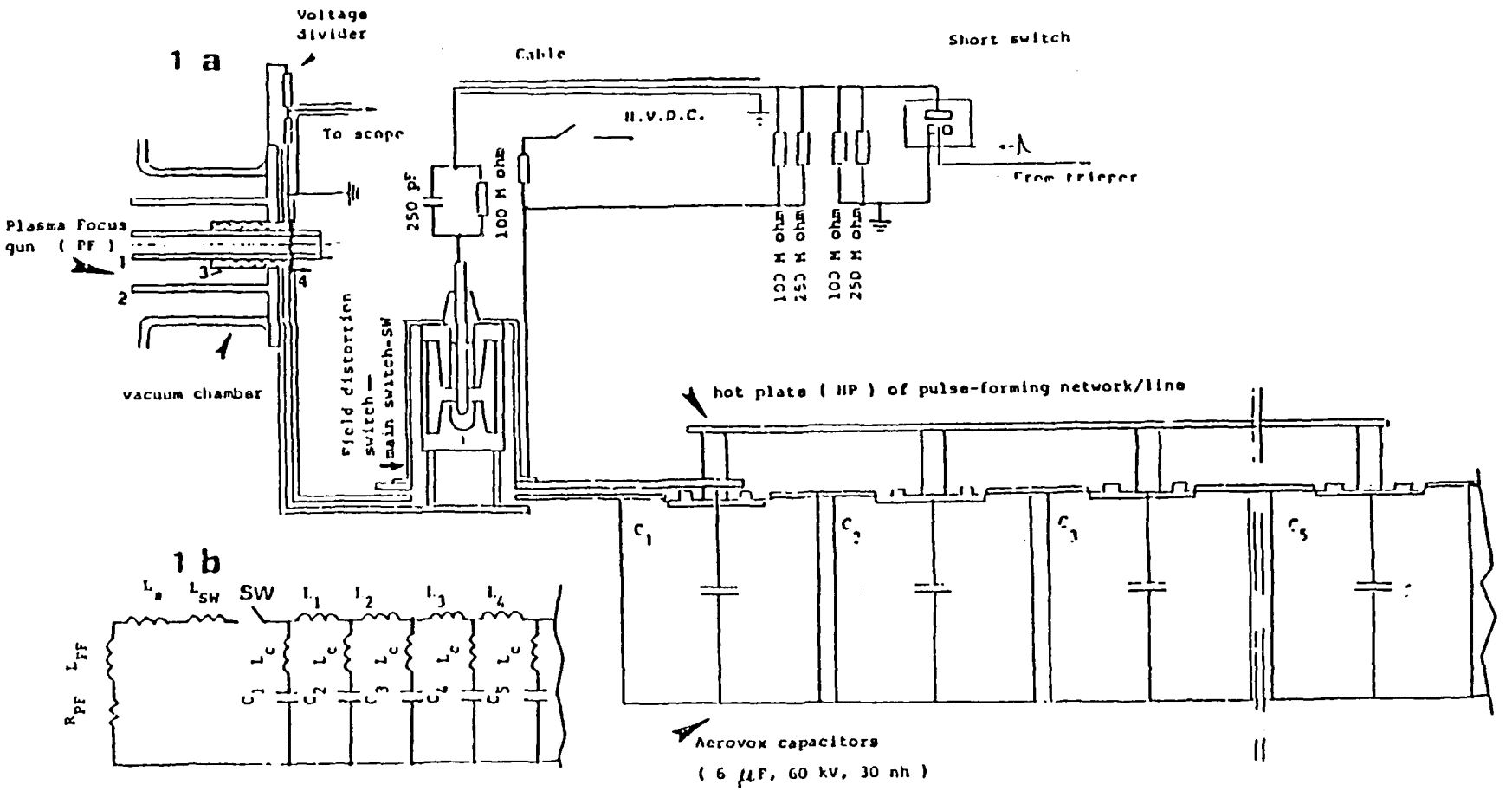

L_{PF}=15-20 nh, $L_s + L_{SW}$= 55-50 nh, L_c=30 nh

$L_1 = L_2 = L_3 = \ldots = L_i$ = 240 nh, $C_1 = C_2 = \ldots = C_o$ = 6 microfarad

Fig. 2: (a) Oscilloscope display of the current (I) pulse from the ten capacitor network charged at V_0 = 16 kV (the positive direction of the I axis points downward only in this oscilloscope trace; in all the following traces the positive axis direction is upward). This signal is obtained from the time integration of the signal ($V \propto dI/dt$) of the voltage divider 5 (during this discharge the PF electrodes have been shorted with a metallic disc attached at the two electrodes at the muzzle; consistently L_{PF} is, in this case, a constant). Measurements of dI/dt during normal operations of the PF (i.e., no metallic short between electrodes) are made with a Rogowski coil encircling the center electrode at the breech (betwen the two back plates of the PF) and also with a single loop magnetic probe in the same location.
The dip in the middle of the current pulse (and the current reversal) is due to the limited number of elements in the network (N_c= 10) and of $L_c > 0$.

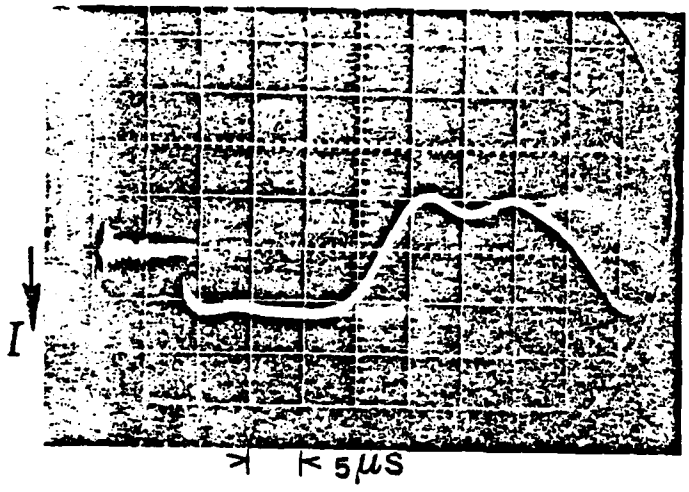

Fig. 2-(b): PF Rogowski coil signal ($\dot{I}$) and X-ray detector signal ($\dot{X}$) -lower trace- from Pilot-U plastic scintillator and photomultiplier (Pilot-U thickness 0.1 mm, smaller than neutron mean free path). All capacitors have been detached from the network but one, the closest to SW (V_o = 30 kV, p = 4 Torr, Max I ≅ 150 kA, n = 1.9×10^8); only one pinch occurs in this discharge (both traces from the same discharge; shot 166). Both traces off scale: 100 V/cm upper trace, 0.2 V/cm lower trace. A knife edge was inserted on the insulator (L_{ke} = 7.5 mm; white dashed lines are used to show trace location in portions of display where trace luminosity was low).

-(c): $\dot{I}$ (in lower trace) and integrated signal I (in upper trace) from the same Rogowski coil signal (time constant of integrating circuit 1 millisec). Five capacitors are attached to the network(N_c = 5) (V_o = 30 kV, p = 2 Torr, Max I ≅ 150 kA, n ≅ 0), this is an example of P_2 type pinches which occurs seldom when a knife edge (L_{ke} = 7.5 mm) on the insulator is used. The second and eighth pinch are the strongest. Note that first pinch occurs after ≈ 1.7 μs after onset of discharge, i.e., the first current sheath travels in the interelectrode gap at a speed v_p smaller (by ≈ 10%) than the speed of the single current sheath in Fig. 2-6, in spite of the smaller value of the filling pressure in this discharge (shot 92).

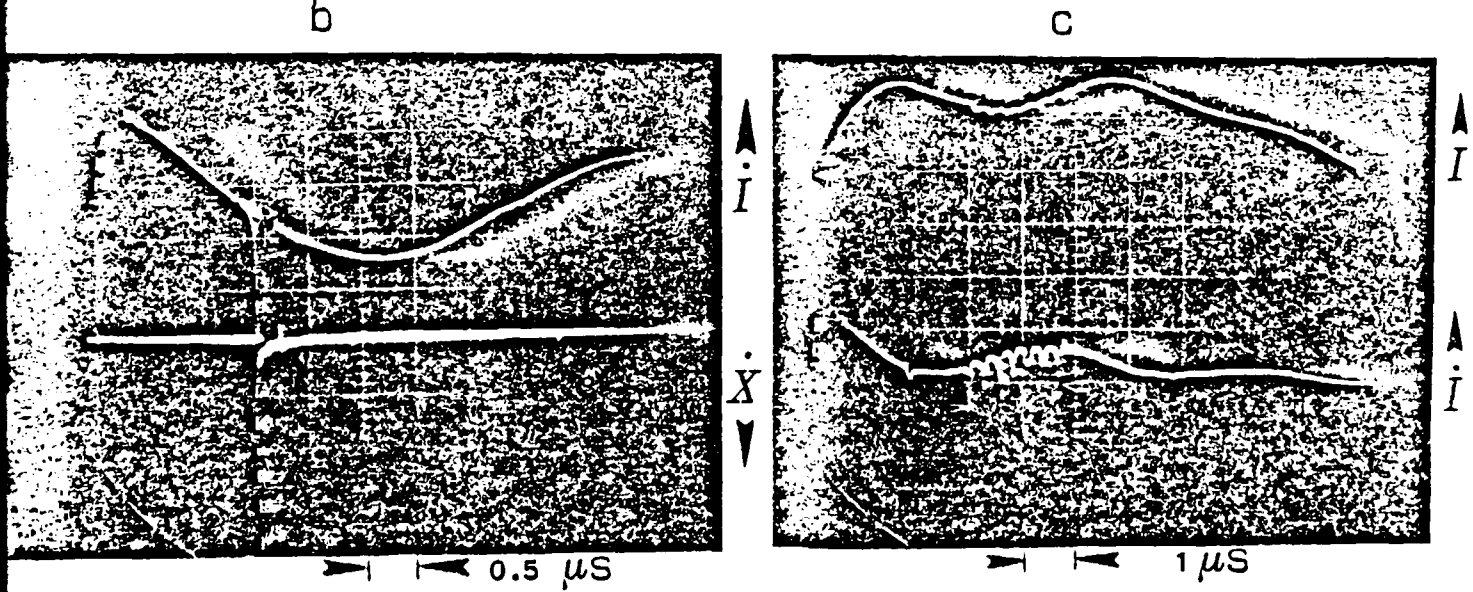

Fig. 2-(d_1): Interelectrode voltage (V) at the breech of the PF from a voltage divider (V-divider 5 of Fig. 1-c) in upper traces, left (shot 57) 2 V/cm and right (shot 58) 5 V/cm. Corresponding $\dot{I}$ from Rogowski-coil signals in both lower traces, (same shots) 100 V/cm; 1 microsec/cm in both displays. In both discharges V_0 = 30 kV, p = 2.5 Torr; n = 3×10^7 for shot 57 which is an example of type P_1 of multiple pinches(first pinch strong, second and third pinches very weak); n = 0 for shot 58 an example of type P_2 pinches. Note weak first pinch of shot 58 which occurs ≈ 600 ns later than first pinch of shot 57 with respect to onset of discharge. Some of the 11 pinches of shot 58 are stronger than the first pinch of shot 57. No knife edge was inserted in these two discharges (N_c = 5).

(d_2): $\dot{I}$ (uppertrace) and corresponding x-ray signal ($\dot{X}$, lower trace), same detectors as in Fig. 2-C (white arrows mark peaks of signal). Three x-ray peaks are detected in shot 176 (left, n = 3×10^7), only one peak in shot 175 (right, n = 5×10^7). Pinch somewhat earlier (by about 200 ns) in shot 175. Both shots are examples of type P_1 of multiple pinches (V_0 = 25 kV, p = 4 Torr, N_c = 5 for both shots, 100 V/cm upper trace, 0.2 V/cm lower trace, 1 ns/cm for all four traces).

d_1

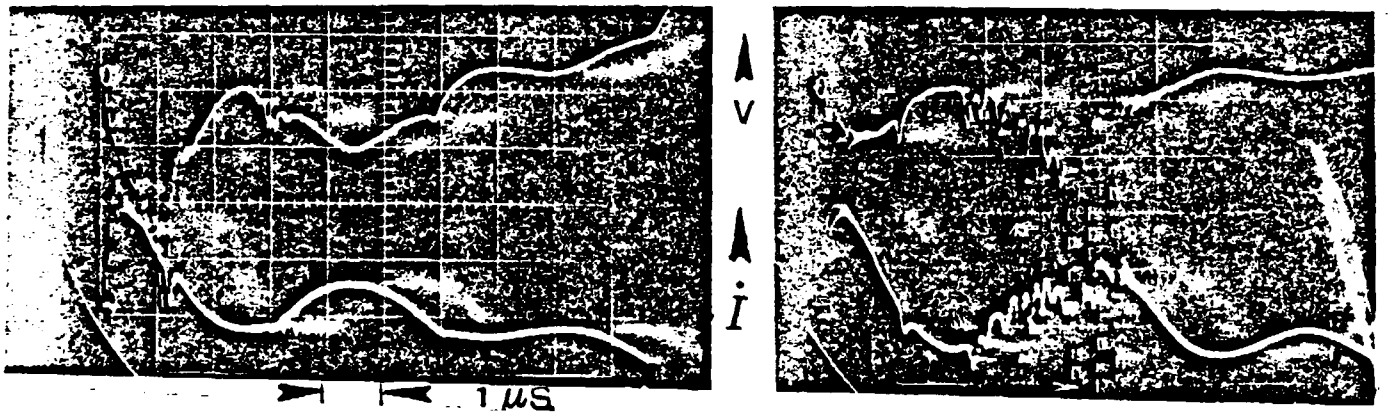

d_2

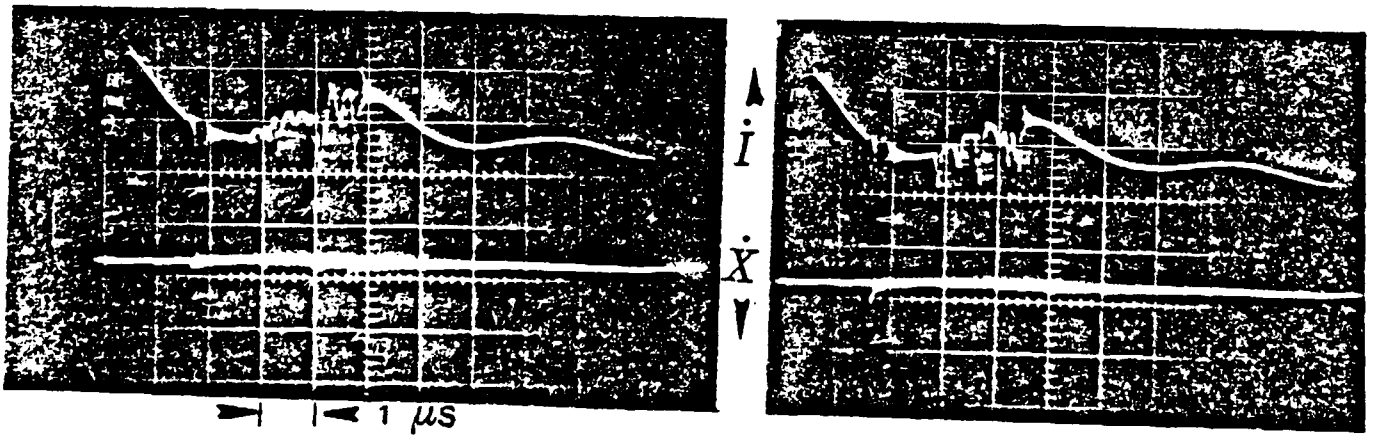

Fig. 3 View of the 200 kJ plasma focus machine of Stevens Tech: (1) discharge chamber; (2) power transmission plates connecting the two rear (penthagonal) plates of anode and coaxial cathode to the five modules (with four capacitors each) which power the machine; (3) the five modules of 40 kJ each are also at the rear of the machine. The five closing switches(one for each module) are hidden behind the power transmission plates (of length two yards) where they connect to the five header plates (4) one on top of each module; the base (5) of the switch is visible under the header plate of the two modules on the left; each high-pressure field-distortion switch can carry about 1 MA. A module header plate (with apertures for connections with capacitors and switch) is on the floor at left(6).A 12 kG magnet for the high resolution ion analyzer (M) is at right. The 10" diameter pump with pyrex connector to the discharge chamber is on the front side(7).

Fig. 4 Discharge chamber of the 200 kJ plasma focus. The anode (center electrode) is a hollow pipe of diameter 10 cm. The cathode is formed by a circular array of 32 stainless steel bars. Both electrodes are visible through the port (during the plasma focus operations a metallic screen covers the internal wall of the port window).

Lt Col Bruce L. Smith	202-767-4994	NP

DD FORM 1473, 83 APR EDITION OF 1 JAN 73 IS OBSOLETE.

SECURITY CLASSIFICATION OF THIS PAGE

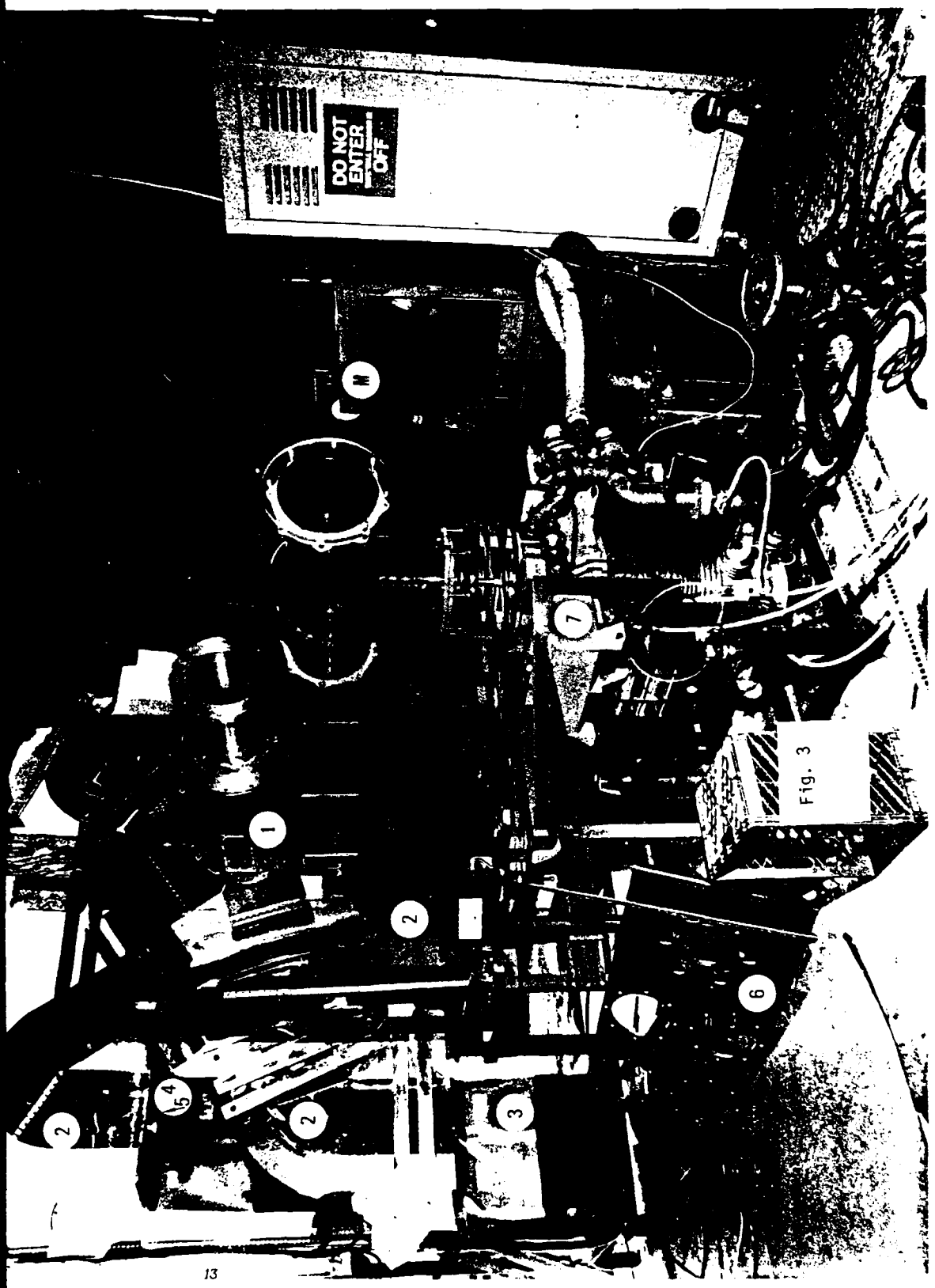

Fig. 3

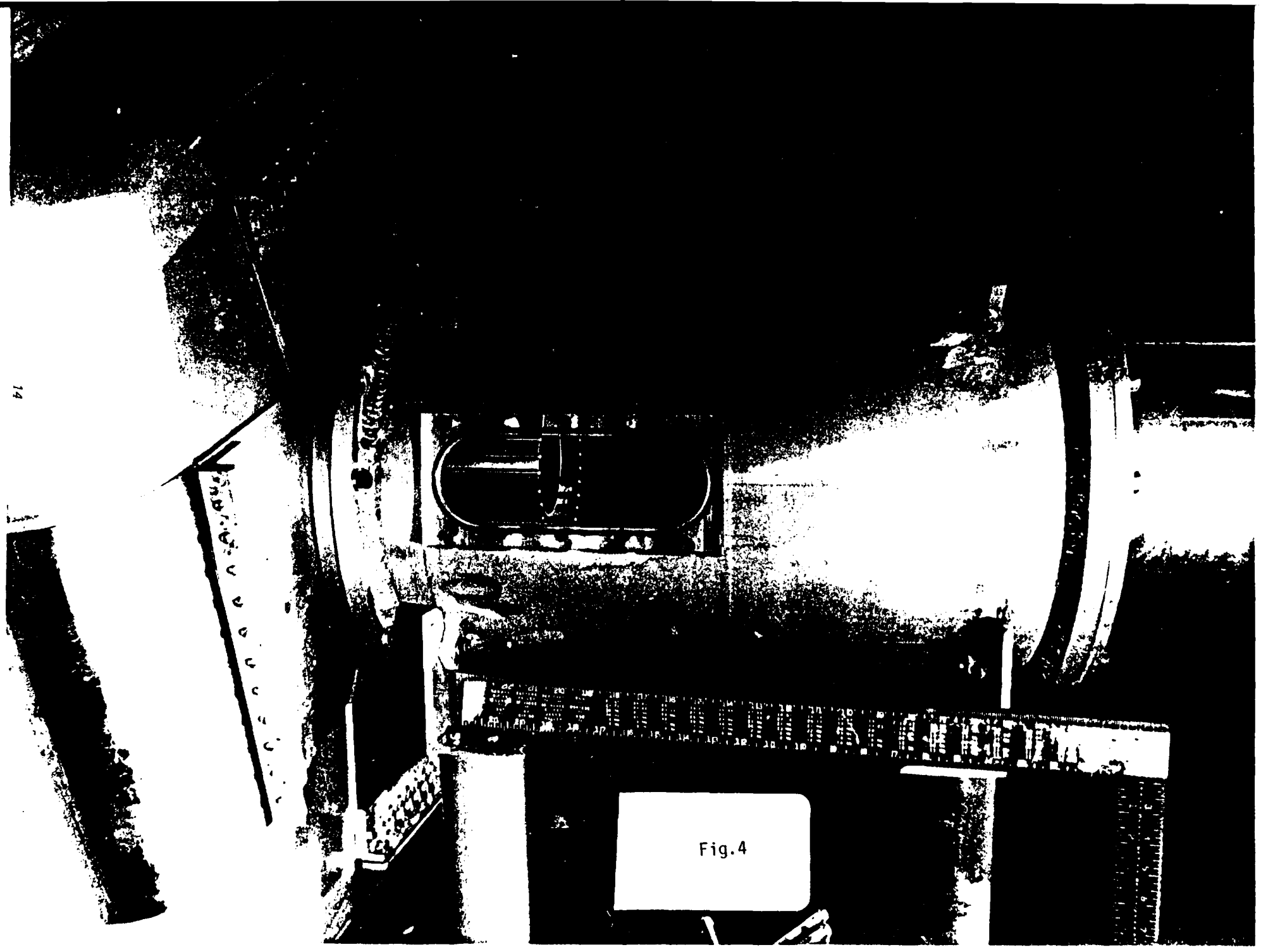

Fig.4

Fig. 4 -(a) Schematic view of the basic element of the MA opening switch (PF coaxial electrodes, with insulator sleeve and different types of field distortion elements in the interelectrode gap). The configuration of the axially pinched current sheath is outlined in the "muzzle" region. The anode side of the current sheath propagates inside the hollow anode after the 4 mm dia. pinch is formed. The best performance is obtained with a knife edge 7.5 mm long at the breech side. In the numerical calculationswe have used knife edges with a triangular cross-section (2 mm high, on the breech side); see Addendum I and II.

-(b) Cross-section of modified knife edge for tests on reduced particle emission from the pyrex surface (figures in mm). Electrode (outer electr., cathode,dia. 10 cm, anode dia. 3.4 cm) and pyrex sleeve dimensions are those of 6 kJ (45μFcapacitor bank, single shot operation) PF .

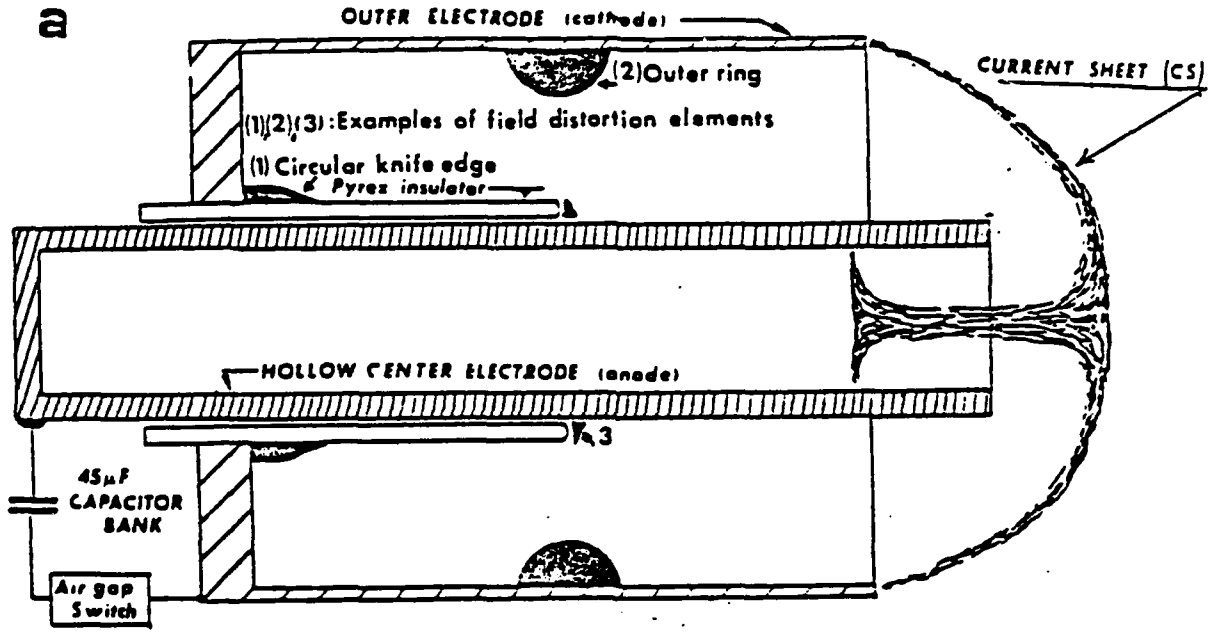

Boundary conditions for the numerical calculation reported in Fig. 4-(c). Different values of the knife edge (ke) length L_{ek} have been tested numerically and experimentally: L_{ek}= 3, 7, 12, 17 mm. Two additional inserts (2, 3) have been used in the numerical calculation , simultaneously with the ke at the breech of the PF (the field distortion of 2, 3 do not substantially interfere with the field distortion of the ke(1)). No appreciable variation of the neutron yield is observed with (2, 3). In all experimental tests only one of the elements 1, 2, 3 was used in one discharge at one time.

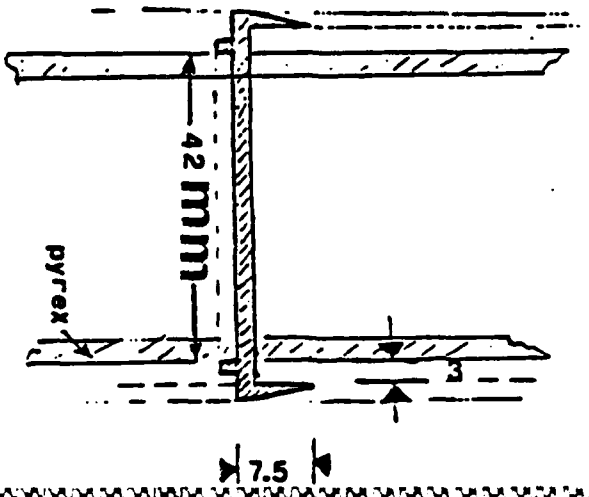

Fig. 4 -(c) Vector plots of interelectrode static electric field (i.e., before breech breakdown) from numerical calculations: (I) None of the field distortion elements is inserted. (II) Knife edge (ke) of length L_{ke} = 7 mm (and elements 2, 3) inserted; with ke the axial (Z) component of the electric field has higher values and extends on a region wider by a factor 2 than the z-component region without ke.

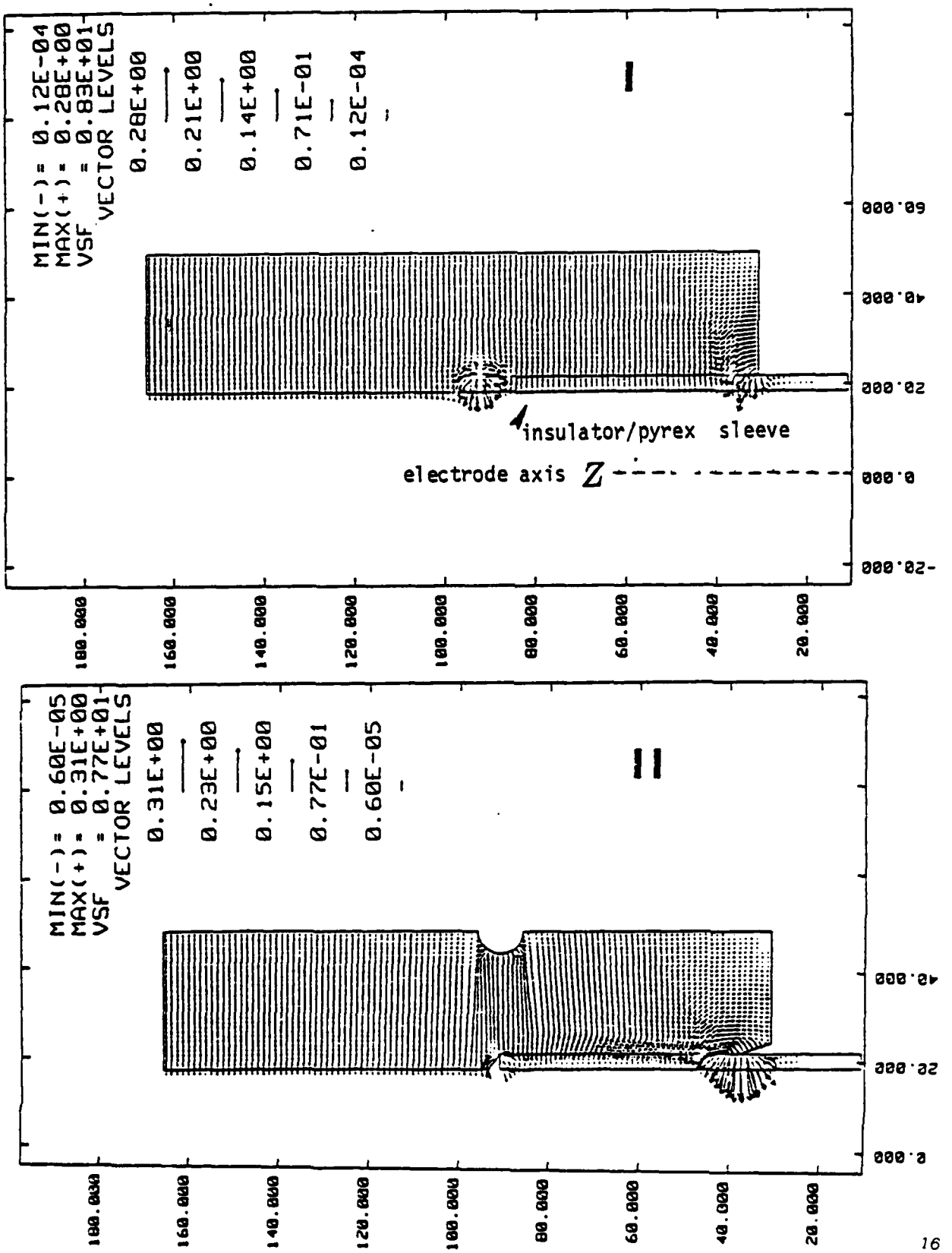

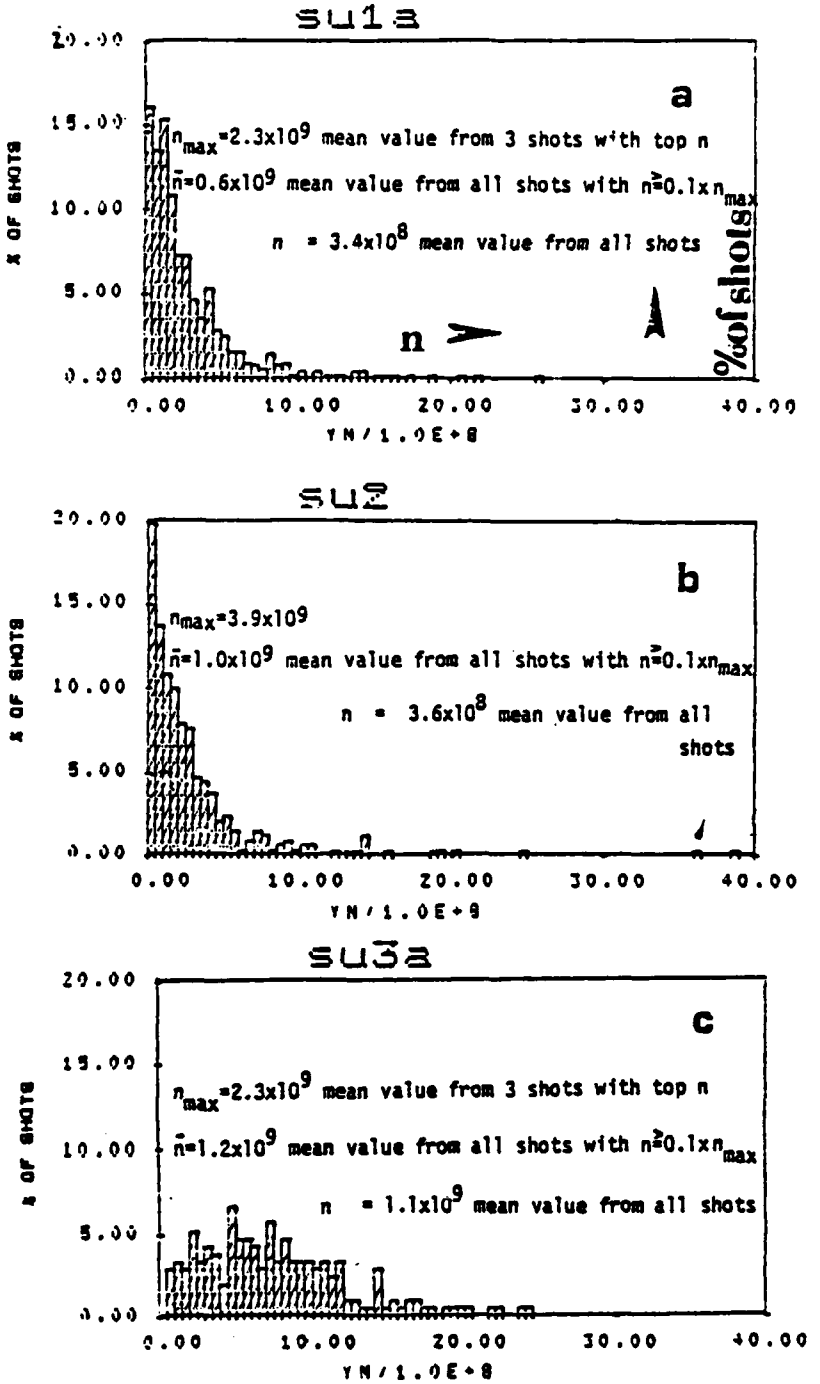

Fig. 5 Histograms with the percentage of shots with a neutron yield between n and n+Δn (Δn = 5x10^7) vs. n for three different initial configuration of the electric field in the interelectrode gap: (a) no ke; (b) ke touching the insulator surface; (c) ke with same length L = 7.5 mm but with a spacing between insulator surface and ke inner surface. The distribution of the data is substantially changed in (c) as compared to (a), (b) in that the misfirings are almost completely eliminated. Both (b) and (c) indicate a substantial increase of n and of $\bar{n}$ with a record yield of n ∿ 3.8 x 10^9/shot. All shots in the same conditions: p = 6 Torr, V_o = 16.5 kV.

Fig. 6. Schematic of the cable-discharge system (via a Kryton tube) for generating the stepped-voltage component $V_p(t)$ on the Thomson spectrometer electrodes in (a). Typical stepped voltage $V_p(t)$ on the spectrometer electrodes -and on the oscilloscope display-in (b), used to obtain the distorted (stepped) sequence of parabola segments of the ion track-pattern in (c); the voltage V_p is decreasing with time;exposure of the target to a single plasma-focus shot (at 0°) with the electric field E_T applied to the electrodes (Max E_T = 5kV/d; d = 4.5mm is the spacing between the spectrometer electrodes which also generate the 5kG field) . The vertical ion-track pattern is obtained from a different shot in which the electric field is turned-off. (d):same as (c) but with a double exposure. After the first exposure the same electric-field strength-but with opposite sign -is applied on the spectrometer electrodes to check reproducibility (D-D neutron yield $y_n \sim$ mean value in both shots). (e) reports the distorted parabola obtained with a periodic electric field (Ref. (f) reports the typical stepped voltage on the spectrometer electrodes described in (b).

Note the double pattern , from two D^+- ion pulses (1, 2) for the same value of the momentum per unit charge P/Z on the left pattern as indicated by arrows 1, 2 on the photograph of the CR-39 target in (d). Time spacing between these two pulses(of comparable intensity in the same spectral region)is 3-5 ns. (Target T-DZ-22A; single shot mode of operation of the plasma focus with a 4 kJ-at 17.5 kV- capacitor bank; $Y_n = 4 \times 10^8$ neutron/shot; 4 Torr of D_2 filling). The first strongly-marked V_p-voltage step (lower side of the track pattern on right and left pattern) is actually the second step of the applied voltage $V_p(t)$. The first step in time can be detected by inspection of the low portion of the track pattern of relatively-weaker intensity, at higher values of the D^+ enargy. The absolute time of a stepped reduction in V_p is measured from the time of the sharp peak in the time derivative (dI/dt) of the plasma-focus-electrode current I - from the signal of a Rogowski coil near the main switch - (at this time , t=0, the explosive disintegration of the pinch is triggered by a surge of anomalous resistivity); this signal is used to start a ns discharge of a high- voltage cable(trough a kryton tube) connected to the Thomson-spectrometer electrodes. The transition time from one value of V_p to the lower step (via voltage-pulse reflection at the cable termination) is 5 ns. A maximum of time resolution is achieved during this transition time .

ϑ_E, ϑ_B indicate electric-field and magnetic-field- induced deflections,respecti

Fig. 6 a

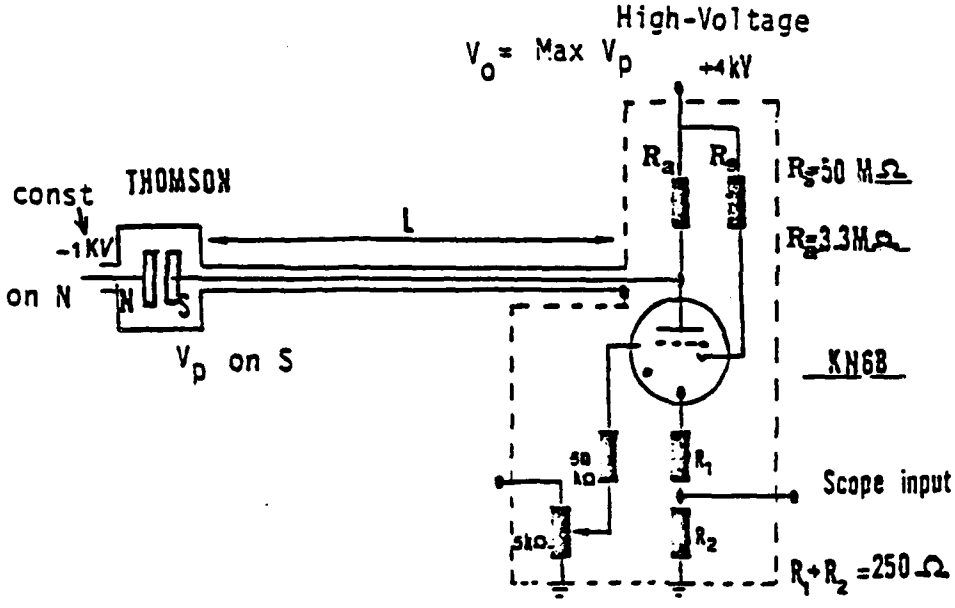

b

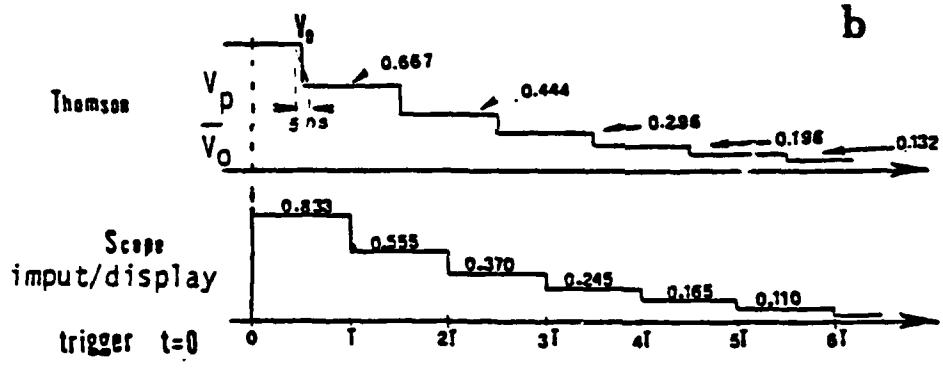

L = 2.5 m

CABLE: Z_o = 50Ω T = 25 ns (=2L/v)

v = 20 cm/ns (velocity of propagation of voltage pulse in L)

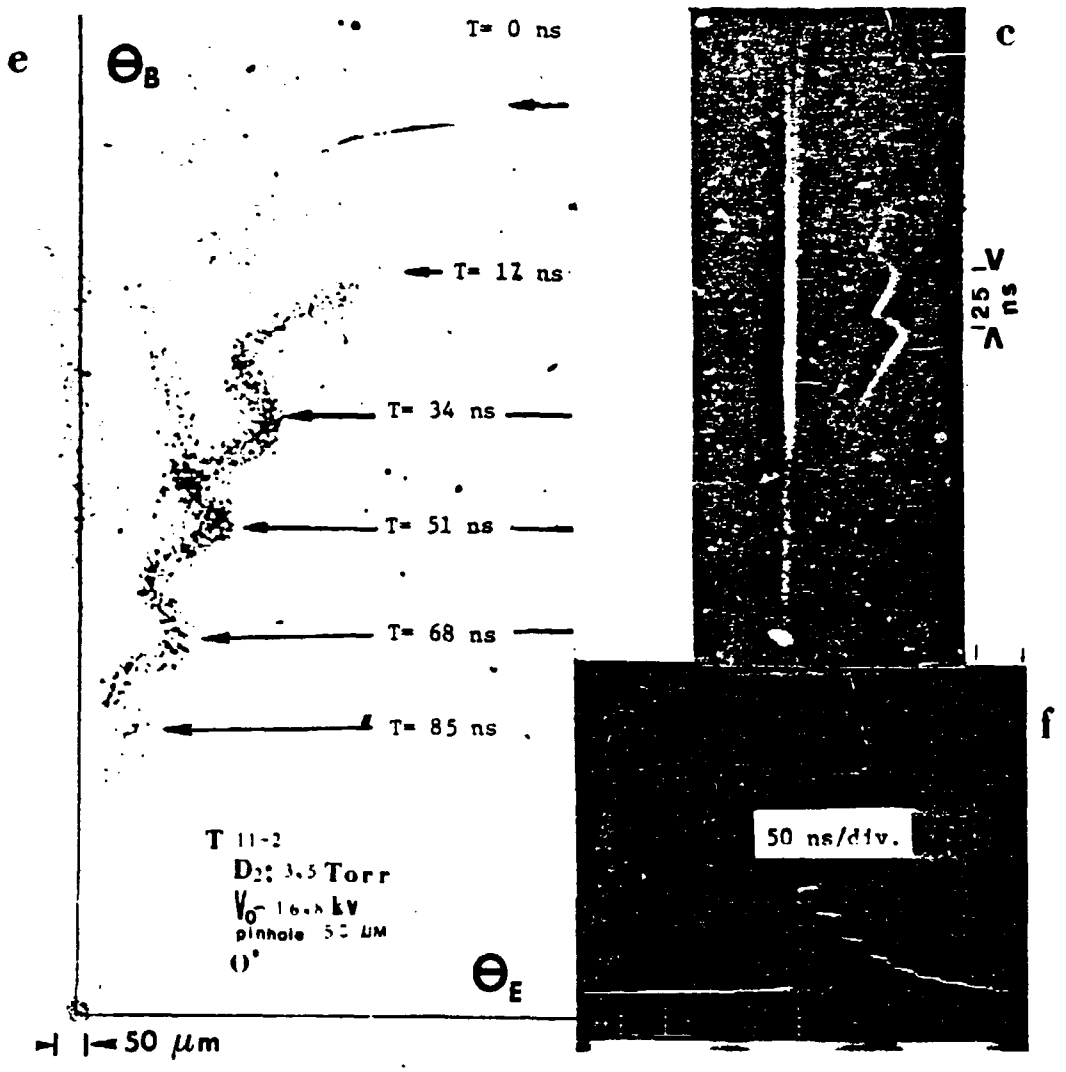

(Fig. 6 d on following page)

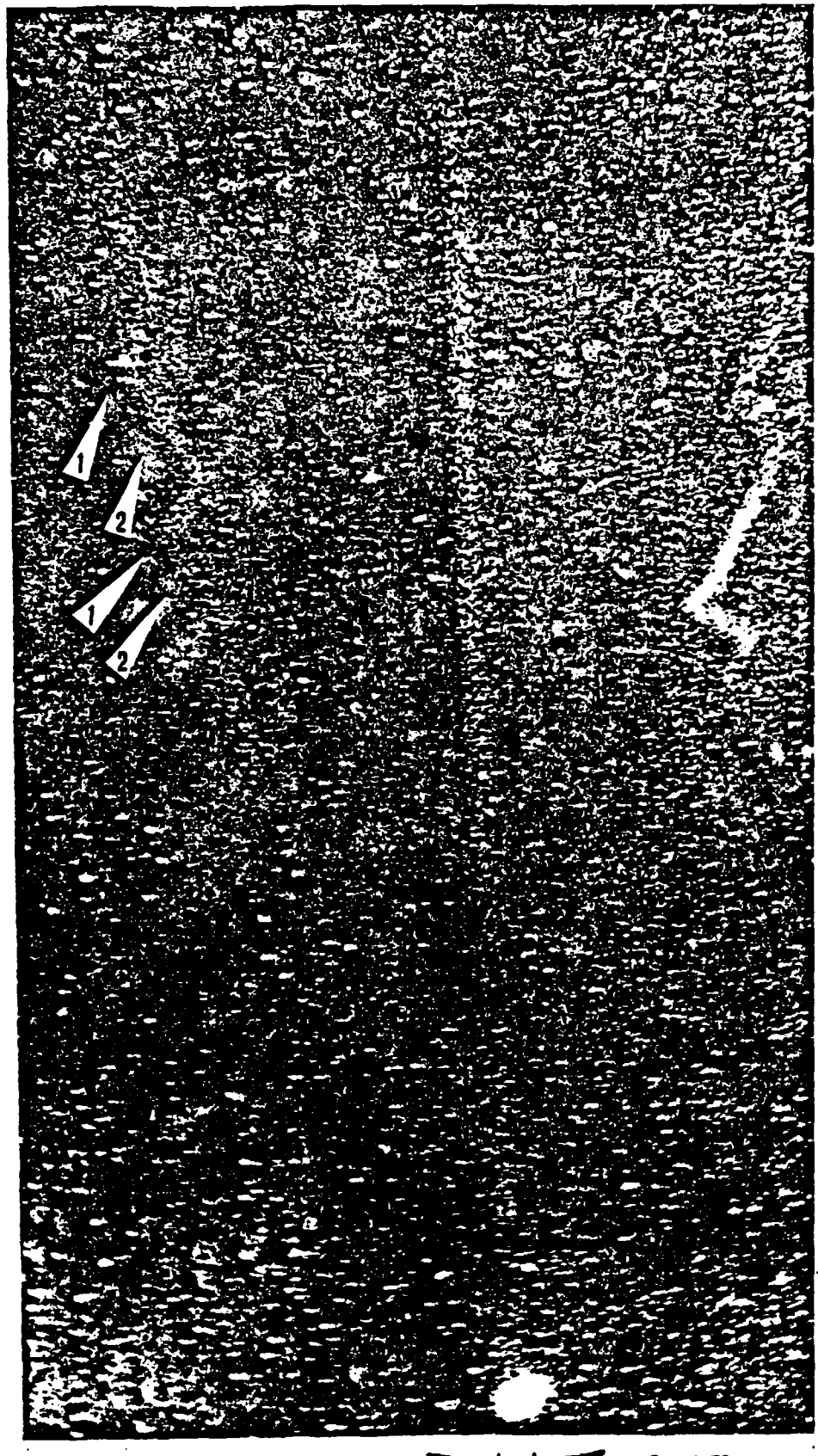

100 μm

neutral point (diameter = pinhole dia.)

impact area of neutral partcles

Fig. 6 - g : Typical delay time (time lag) in the emission of D^+ ions from the exploding pinch (emission in the 0^o direction along the electrode axis)as a function of the ion energy E_i. The low-energy ions are emitted at an earlier time than higher- energy ions. The relative time of emission is obtained by comparing the difference between time of impact on the target and time of flight(known from the ion energy and the distance source-target) . The"absolute"time of emission is determined with respect to the peak in the current drop on the electrodes(surge of anomalous resistivity in the pinch). The typical time of emission of the ions with E_i = 200 keV is about 50 $\pm$ 10 ns after the time of peak in the electrode current drop.

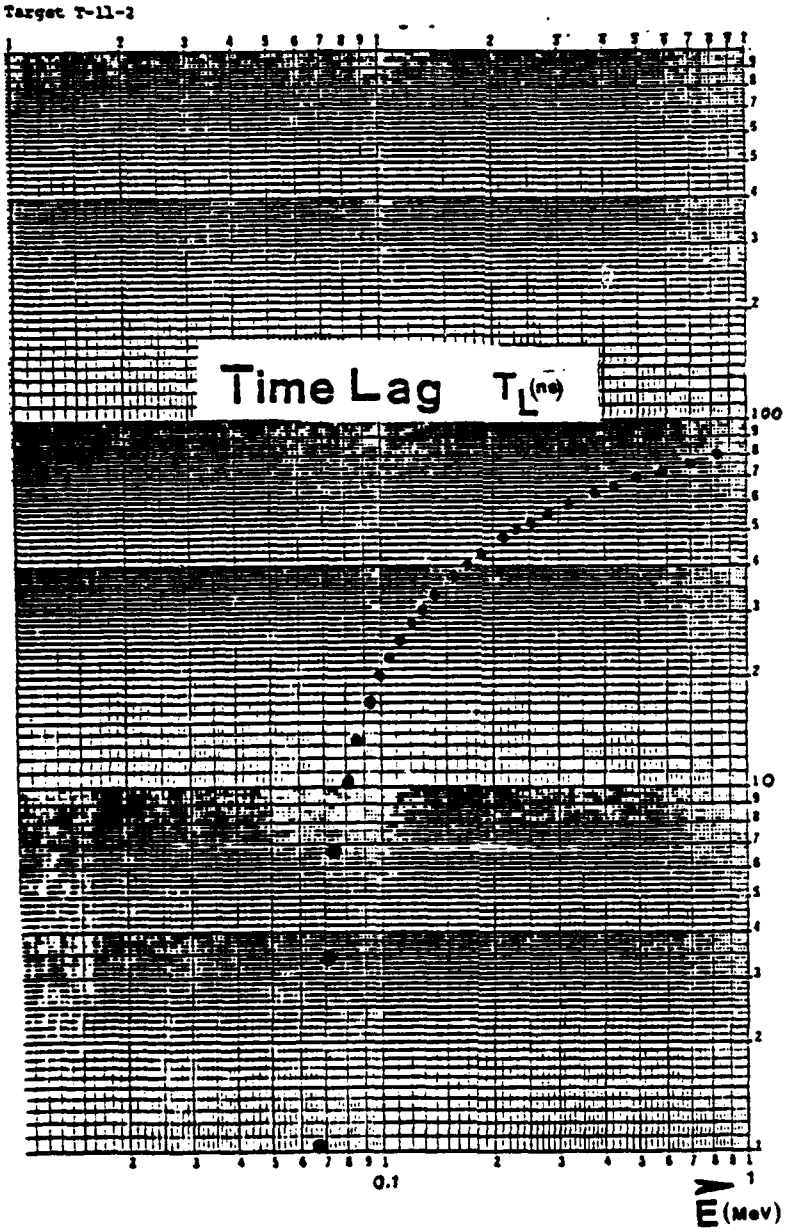

Appendix 1

HEAVY ION FUSION IN A DENSE PINCH WITH ENHANCED COMPRESSION, ION ACCELERATION AND TRAPPING

High space resolution imaging with a pinhole camera of the plasma focus pinch (from X-ray and particle emission) indicates the existence of localized hot spots which are the source of the hard component of the pinch emission (> 3 MeV D^+ ions and > 10 keV X-rays)[1-4]. These hot spots (with typical linear dimensions of 10-200 μm) are embedded in an extended, diffuse source of softer radiation (X-rays, ion and ion clusters) which form the profile of the plasma focus pinch. The hot spots are clearly linked to the filamentary fine structure of the pinch from X-ray pinhole images which show space correlation and overlapping of those elements of the pinch fine structure.

We present here independent data which supports the ubiquitous nature of these elements of the pinch fine-structure.

Important information about plasma hot spots which are the site of high nuclear reactivity and of the acceleration, confinement and/or emission of high energy ion beams (HEB, say) has been obtained from (d,n) nuclear reactions involving heavy nuclei ($A \simeq 15$)[5]. During our experiments the discharge chamber of the advanced plasma focus (APF, say) fed with a 7 kJ (at 17 kV) capacitor bank was filled with a suitable mixture (e.g., D_2 and N_2 or D_2 and C_3D_8) with an atomic ratio, r, of heavy nuclei as large as r = 0.15/1. The β^+ radioactivity of the reaction products in the gas was measured after each APF shot and, at the same time, we have observed the β^+ radioactivity from (d,n) reactions in solid external targets of ^{10}B, ^{12}C, ^{14}N, ^{16}O (axial, 0°, and side-on, 90°, directions).

The "effective" D^+ energy, E_e, fitting the observed amount of each of those reactions is $E_e > 2$ MeV if we take the D^+ energy spectrum of the form $\partial\phi/\partial E = \phi_0 E^{-m}$ with $m = 2.5 \pm 0.5$ and ϕ_0 as determined from the observed D-D neutron spectrum and other data[5]. Special precautions were taken for a correct identification of the reaction products in the gas and in the solid targets. From the observed β^+ radioactivity of each species in the plasma and in the external targets (in the same shot) we determine the (d,n) reaction yield, Y, of each reaction; the measured neutron yield, Y_n, provides the yield of the $D(d,n)^3He$ reactions. Our data from many shots indicate: (i) a linear correlation among all measured yields Y's of the heavy ion reactions; (ii) functional dependence $Y \sim Y_n^2$ on the neutron yield. For a specific reaction the measured ratio of the yield in the plasma, Y_p, and the yield in the external target, Y_{ET}, in the same shot can be equated to the analytic expression, i.e.,

$$(Y_p/Y_{ET})_{exp} = (n\tau \cdot r/(r+1)) A \cdot \int(\partial\phi/\partial E)\sigma E^{0.5} dE / \int(\partial\phi/\partial E) y a dE \qquad (1)$$

In this equation the only unknown quantity is nτ, n-is the total density of nuclei in - and τ is time of the HEB transit through- the plasma target. A - is a unit dependent constant, a-accounts for the β^+ selfabsorbtion in the external target, $y(E) = \int \sigma(dE/dx)^{-1}dE$ is the experimental thick target yield of a monoenergetic beam , σ-is the (d,n) reaction cross-section. In the integrals the lower limit is the reaction threshold energy and the upper limit is the highest observed energy of the ejected D^+ HEB, i.e., = 10 MeV.

From Eq. (1) we find $3 \cdot 10^{12} cm^{-3}s \leq n\tau \leq 1.2 \cdot 10^{13} cm^{-3}s$ from shots with $Y_n \simeq 10^9$, independently on r, for all reactions with ^{12}C, ^{14}N in the plasma, and ^{10}B, ^{12}C, ^{14}N, ^{16}O in the solid external targets. The uncertainty in the determination of nτ depends on the detector geometry, the accuracy of the cross-sections and the relative fluctuations of the β^+ activity for a specific value of Y_n. By taking an "effective" life-time of HEB (inside the reacting plasma region, possibly a multiplicity of hot spots) equal to τ = 25 ns (where τ is the FWHM of our neutron emission signal from an NE-102 scintillation detector) we find $1.2 \cdot 10^{20}$ $cm^{-3} < n < 4.8 \cdot 10^{20}$ cm^{-3}. This value of n (a minimum value estimate) contradicts the value from usual density measurements ($n_{exp} = 5 \cdot 10^{18}$ cm^{-3}) with a 2mm spatial resolution [6]. Alternative attempts of explaining the observed high value of Y_p/Y_{ET} (specifically $Y_p/Y_{ET} = 0.03$ for $^{12}C(d,n)$ ^{13}N with r = 0.15 in the filling mixture) fail as: (a) the assumption of an anomalous concentration of the heavy nuclei with an increase of r in the hot spots, above the initial value of r in the filling gas, decreases the reaction-fitting value of n by factor = 4 for the heavy ions but simultaneously decreases far Y_n by a factor ~ 3 in contradiction with the observations, (b) the assumption of a significant slowing down-over extended plasma regions-of accelerated D^+ ions from the hot spots changes Y_p/Y_{ET} but it requires (for an estimate of Y_n consistent with the measurement) an HEB population of such a ignitude (via ϕ_o) that it would exceed the capacitor bank energy (the D^+ slowing-down time would also be too long, i.e., about 3 times longer than neutron signal FWHM).

Since no valid alternative is found to the picture of high-density hot spots where the bulk of the nuclear reactions takes place we conclude that the heavy-ion reaction yield is an excellent supporting argument in favour of the hot-spot existence and leading role. The validity of the concept of high-density hot spots requires that the hot-spot dimensions are small enough for not significantly contributing to the direct measurements of n with space resolution of = 2 mm. By assuming that a multiplicity of hot spots can change n not more than 10% (the experimental uncertainty in a direct measurement of n) we estimate a hot spot diameter of about 100 μm, in agreement with our direct experimental observation.

The pinhole image of the pinch from particle emission is recorded on a CR-39 target (with suitable ion filters) where the nonuniform distribution of etched tracks of ions and ion clusters indicates that some of the localized sources of D^+ ions with energy 2-4 MeV have dimensions smaller than the pinhole diameter = 100 μm. The small dimensions of the localized sources and the extreme collimation of the ejected HEB's of microscopic diameter are consistent with an accelerating - field intensity of = 1 GV/cm. A compression in the HEB time of emission which is similar to the space compression of a localized HEB source is revealed from time

Fig. 2. Zero degree pinhole image of the plasma focus pinch. The central figure shows the typical diameter of the HEB (= 1.5 MeV of D^+) ejected at 0^o . Some magnification for 1,2,3,4,5,6 reporting details of center photograph; #1 reports ion tracks of central spots behind 25μm mylar screen.

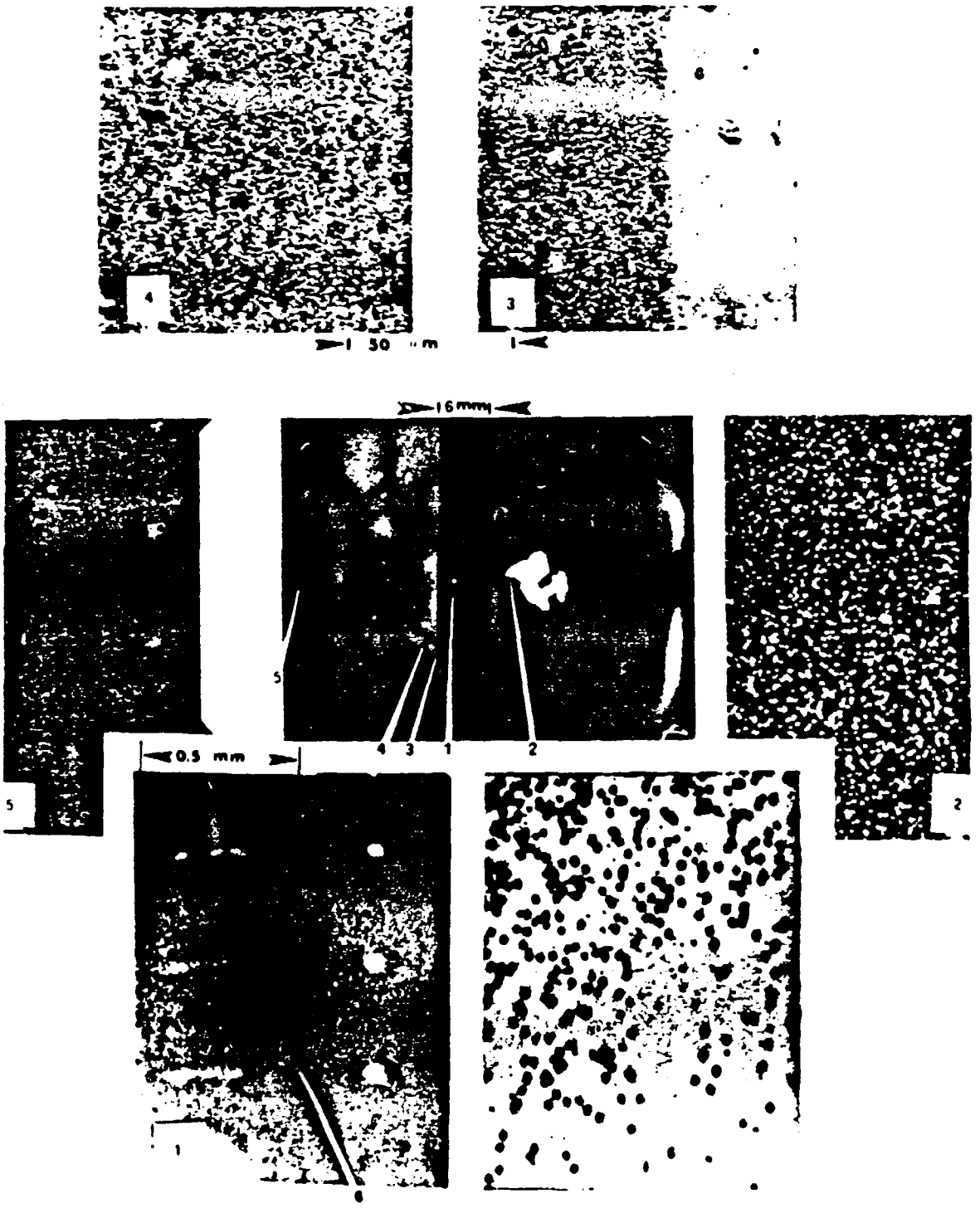

resolved Thomson spectrometer data (the duration of the ion pulse is shorter the higher is the ion energy; e.g., slow ions, 100 keV D^+, are ejected 50 - 100 ns earlier than 1 MeV ions)[5,7] . An increase in the quantity of these hot spots (with a consistent increase of the neutron yield Y_n and of the heavy-ion reactions in the pinch) was obtained in our experiments with the insertion of suitable field distortion elements in the interelectrode gap. This establish the possibility of controlling and increasing the amount of hot-spot activity for a variety of practical applications.

*Work supported in part by AFOSR, ONR (USA), CNR, MPI (Italy).

REFERENCES

1. W. H. Bostick, V. Nardi, W. Prior, J. Plasma Phys. 8, 7 (1972).
2. V. Nardi, C. Powell, A.I.P. Conf. Proc. 111, p. 463 (1983).
3. V. Nardi, "Megagauss Technology and Pulsed Power Application" Ed. C. M. Fowler, Plenum Publ. Corp. 1987, p. 269.
4. M. Sadowski, et al., Phys. Letters 113A, 25 (1985).
5. V. Nardi, et al., IEEE Trans. on Plasma Science (to be publ. June 1986).
6. H. Herold, et al., IAEA-CN-44/D-III-6-3 p. 579 (1985).
7. V. Nardi, et al., European Conf. Abstracts 11D part II, p. 548 (1987).

Fig. 1. Pinhole image of the pinch from the nonuniform distribution of etched ion tracks on a CR-39 target (pinhole diameter 150 μm). The V-shaped image of the pinch is caused by a 5 kG permanent magnet inserted behind the pinhole, between the pinhole and the target; the electrodes are at the left. The magnet induces the splitting of the pinch image by deflecting the D^+ ions but it is not affecting the trajectory of the heavy clusters with $z/m \cong 0$. The clusters at the right disintegrate later than the cluster at the left. Note diffuse image of hot plasma, emitting a relatively small fraction of neutrons (≈ 30% of total).
The lower part of the V-shaped image along the horizontal electrode axies is formed from the heavy clusters.The focalization of the current reaches a maximum at the right side - this pinch region with a maximum of current density ejects clusters with a longer life time.

Stimulated Acceleration and Confinement of Deuterons in Focused Discharges (Part I)

V. NARDI, A. BORTOLOTTI, J. S. BRZOSKO, M. ESPER, C. M. LUO, F. PEDRIELLI, C. POWELL, AND D. ZENG

Abstract—**Acceleration and confinement of megaelectronvolt D^+ ions in the plasma focus (PF) are analyzed in terms of the observed energy spectrum of the ejected ions and of the energy spectrum of the D–D neutrons from which the trapped-ion spectrum is derived. The current distribution in the interelectrode gap can be modified by field distortion elements (FDE's) which increase the fraction of the total electrode current flowing in the pinch. An optimized FDE increases the observed maximum value, Max Y_n, and the mean value $\bar{Y}_n$, of the observed D–D neutron yield per shot Y_n by a factor ≥ 3. The ejected-ion spectrum is determined by three independent methods (Thomson spectrometers, high-resolution magnetic analyzer, filters, and Faraday cups).**

I. Introduction

THE energy spectrum $d\phi/dE$ of the ion emission from a plasma focus (PF) pinch in our experiments has been determined in the ion energy interval $E \sim 50$ keV to 8 MeV with: 1) Thomson (parabola) spectrometers [1], 2) a high-resolution magnetic analyzer with field-edge focusing (our energy resolution is $\Delta E/E \sim 5/1000$ for a D^+ ion energy $\sim$1–4 MeV) [2], and 3) a time-of-flight Faraday cup-filter method [3]. The energy spectrum of the D^+ ions which are trapped in the pinch region is here obtained on a smaller energy interval $E \sim 0.6$–1.5 MeV from the D–D neutron energy spectrum as determined via a time-of-flight (TOF) method [4]. Spectral determinations have been carried out in other laboratories for the trapped ions via the D–D neutron energy spectrum from nuclear emulsions (n/em.) [6] and by a variety of methods [7], [8] (e.g., as those of [1] and [3]) including nuclear activation [4], [9], [10]. These data are mutually consistent if we allow for a rigid translation via a constant amplitude factor A in $d\phi/dE$ which essentially reflects the different energy levels used in PF operations of different laboratories. Methods for increasing the ion confinement time in the pinch region are suggested from a comparison of the spectrum of the ejected ions with the spectrum of the trapped ions, from shot-to-shot variations of amplitude, as well as from the $d\phi/dE$ amplitude variations as determined via a redistribution of the interelectrode current. The fraction of the interelectrode current flowing in the pinch (usually from 50 to 90 percent of the total, depending on PF optimization conditions, energy level, and inductance of capacitor bank and power transmission line) is generally increased by using a suitable field distortion element (FDE), specifically a metallic knife edge (KE, say, of suitable diameter d and length l) which encircles the base of the insulator sleeve. This extends the confinement time of high-energy ions inside a broad region (of diameter ≥ 2 cm) surrounding the pinch, after the axial pinch disintegration, with a tripling of the observed value of $\bar{Y}_n$ in our PF system with a capacitor bank energy $W_0 \cong 6$–10 kJ at a voltage $V_0 = 15$–19 kV) [4]. Information on the megaelectronvolt-ion confinement time is also provided by the amount of 14-MeV neutrons generated from secondary D–T reactions (the tritium is bred by primary D–D fusion reactions in the discharge chamber which is initially filled with pure D_2 gas without tritium) [5], [11].

The coaxial electrode/insulator geometry is of the Mather type [12] (center-electrode/anode diameter 3–6 cm; outer electrode/cathode diameter 10 cm) and has been repeatedly reported in the literature [1], [2], [12].

II. Fusion-Reactions and Spectrometer Data

Systematic measurements of the neutron yield Y_n and of the corresponding maximum value of the neutron energy max E_n detected in the same shot indicate that Y_n is strongly correlated with max E_n: specifically, if we plot Y_n as a function of max E_n, we find that Y_n is monotonically increasing with max E_n as reported in Fig. 1(a) [4], [5].

The observed values of max E_n imply values $E > 1$ MeV within the pinch regions where D–D fusion reactions occur. In Fig. 1(b) we report our observation for a typical series of shots (at 5 torr of D_2, 16 kV) of the ion emission at 45° (of ions with energy 50 keV $\leq E \leq$ 2.4 MeV as it is recorded from etched ion tracks on CR-39 targets. The typical ion-track density is 10^6–10^7 ions/cm^2 at a distance of 15 cm from the pinch axis). These data (but for a few exceptions) indicate an increase of the ion emission, with the neutron yield Y_n up to $Y_n \simeq 2\,\bar{Y}_n$ where $\bar{Y}_n$ is the mean value of the yield over hundreds of shots in the same conditions. For $Y_n > 2\,\bar{Y}_n$ the ion emission

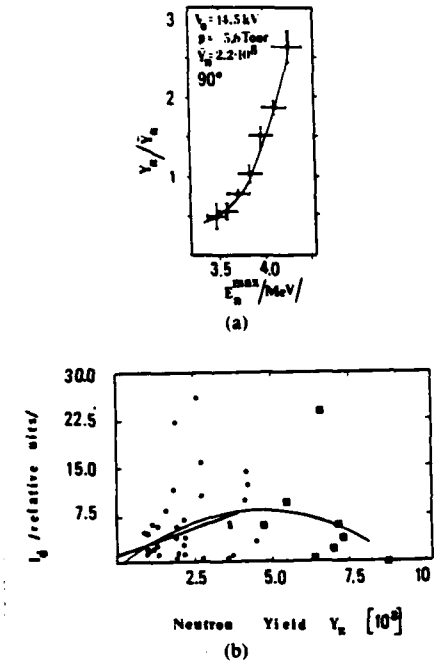

Fig. 1. Y_n versus max E_n (the maximum value of the neutron energy E_n, observed in one shot from a TOF method [5]). Each data point with error bars is generated as the mean value Y_n from a set of 10–15 shots with the same neutron TOF ($T_f \pm 10$ ns) on a distance $L = 1486$ cm between detector and neutron source. $\bar{Y}_n$ is the mean value of Y_n from all sets of shots. These neutron-energy data have been taken in the 90° direction (i.e., side on) with respect to the electrode axis. (b) I_i versus Y_n from D^+ track count on 45° pinhole image of pinch. Pinhole diameter is 150 μm: pinhole is at the same distance (7.5 cm) from source and target. Similar results are obtained from images at 90° and at 0° (respectively, with a somewhat lower and higher count than that from the 45° image). A best fit with a parabola (and with a straight line up to $Y_n \lesssim 2\bar{Y}_n$: data points (■) are not included) is reported. Discharges with FDE (50 percent of the total) and without FDE have been used for generating these data points.

from the pinch region decreases and is below the detectable level when $Y_n \sim \max Y_n$. The data of Fig. 1 are consistent with the view that shots with maximum yield correspond to optimum confinement conditions. The time-integrated ion emission I_i at 45° in Fig. 1(b) is determined from the area S of the pinhole image of the pinch via $\int \lambda \cdot ds$ (where λ = (number of ion tracks)/cm^2 on the element ds of CR-39 target surface where the pinch image is recorded). The pinch image has sharply defined boundaries with a drop of the ion-track density λ by one or two orders of magnitude on a distance < 100 μm at the outer boundary of the image, so that only the area inside the boundary contributes an appreciable amount of $\int \lambda \cdot ds$ (track-forming ions on our CR-39 have an energy 50 keV $\lesssim E \lesssim 1.5$ MeV). We may consider the Y_n of each shot as the result of two interplaying factors: 1) the rate of decay of the magnetic structure of the pinch (a function of location x and time t) which determines ion-accelerating inductive field, maximum value of E, and max E_n, and 2) the confinement (or trapping) time of accelerated ions within the magnetic field of any neighboring region (at a location $x + \Delta x$, say) where the intensity B of the magnetic field still has a high value at a time $\gtrsim t + |\Delta x|/\sqrt{2E/m_i}$. The data of Fig. 1 prove that both these factors are controlling Y_n. Ion "confinement" and "trapping" are used here in two somewhat different contexts. With confinement we mean the limitation of the ion trajectories within the axial plasma column of radius $\lesssim 2$ cm (which includes the pinch) where a large fraction of the interelectrode current continues to flow during a time interval ~ 0.5 μs (in our 6–10-kJ system) starting from the pinch formation time. With trapping we mean the limitation of ion trajectories within any of the elements of the fine magnetic structure of the pinch as the filaments (with a high density of particles and of currents) in the pinch and in the off-axis part of the current sheath between electrodes.

By inspection of the etched-ion tracks on CR-39 targets and differential filters we find that the ion emission is sharply peaked at 0°, with a drop of the fluence $d^2\phi/d\omega dE$ (for $E \gtrsim 3$–500 eV$_0$, e = electron charge) to a fraction $\lesssim 1/10$ of the peak value, at an angle $\theta_b \cong 3°$ from the electrode axis (0° direction). The amount $\int_{\Delta\omega}(d\phi/d\omega)\,d\omega$ of ejected ions inside the solid angle $\Delta\omega \lesssim 8.6 \times 10^{-3}$ sr defined by $2\theta_b$ (the 0° ion beam, by definition) has a hard component formed of a multiplicity of ion streams, each of which is highly collimated inside a solid angle $d\omega \lesssim 3 \times 10^{-5}$ to 1.4×10^{-6} sr in a random direction inside $\Delta\omega$, i.e., in the 0° cone of aperture $2\theta_b$. A similar multiplicity of ejected hard streams (highly collimated ion microbeams, say) is observed in all directions [13] with a fluence minimum at $\theta = 90°$ and a relative maximum at 180°. This distribution matches the angular dependence of the smoothly distributed, soft ($E < 1$ MeV) ion-emission component which contributes to ϕ an amount $\int_{4\pi-\Delta\omega}(d\phi/d\omega)\,d\omega \sim \int_{\Delta\omega}(d\phi/d\omega)\,d\omega$ ($E \gtrsim 50$ keV). The pinhole image of the pinch from particle emission at different angles (90°, 45°, 0°; pinhole diameter 150 μm) on CR-39 plates with differential filters [1], [13] indicates that hard ion streams are generated inside a multiplicity of "hot spots" embedded in the pinch. Some of the hot spots have a diameter—as recorded by the ion-track distribution of ions with energy $E_i > 2.4$ MeV—of about 100 μm, i.e., smaller than the pinhole diameter [1], [13].

Consistent information on ion confinement and trapping is provided by the ion spectrum of Fig. 2. The reported spectrum $d\phi/dE$ of the ejected D^+ ions is simply $d\phi/dE = 4\pi \times d^2\phi/dEd\omega$, i.e., $(4\pi/d\omega)\,x$ (observed ion fluence in the solid-angle element $d\omega$ at 0°). The method of estimating the trapped/confined-ion spectrum from the neutron spectrum dY_n/dE_n is described in Section III and in the caption of Fig. 2. The data at 0° indicate that wide variations may occur from shot to shot also at a fixed value of the bank energy in the $d\phi/dE_i$ amplitude but not in the spectrum shape (this conclusion follows from comparing the spectrum on targets exposed to a single PF shot with the spectrum on targets exposed to at least eight PF shots, each with $Y_n \cong \bar{Y}_n$, as is the case for the target with the data (▼) of Fig. 2). For an assessment of the fraction of confined ions $N_i(C)/N_i(A)$ and of ejected ions

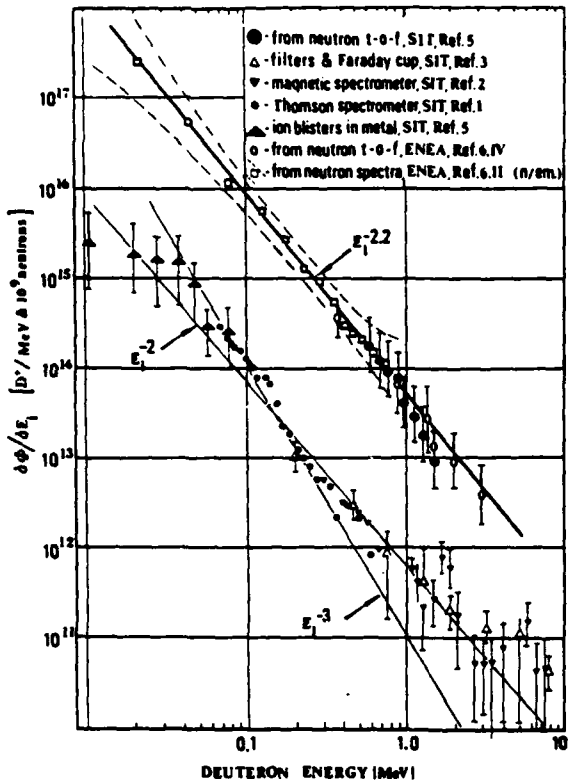

Fig. 2. D^+ energy spectrum $\partial\phi/\partial E$ versus E for ejected D^+ (▲, ▼, △, ●) and for trapped D^+ (○): □, ● from time resolved data. Data from the skin thickness of ion-induced blisters in metals ($=D^+$-range in the metal) covers the range ~ 10 keV to 0.8 MeV. Thomson spectrometer data (from the parabolic pattern of etched ion tracks recorded on CR-39 plastic targets) cover the range 70 keV $\leq E \leq$ 1 MeV. The other two methods cover the range 0.3 MeV $\leq E \leq$ 8 MeV. D^+ spectra from different methods have been normalized to have a minimum-square difference in a chosen E interval. The spectrum from Frascati PF neutron data (trapped D^+) is reported for reference. The amplitude factor is normalized to fit SIT Y_n (10^9 neutron/shot).

$N_i(E)/N_i(A)$ (with obvious definitions $N_i\{A\} =$

$$N_i(C) + N_i(E) \equiv \int_{4\pi} d\omega \int_{E_0}^{\infty} dE d^2\phi_a/dE d\omega$$

where $\phi_a = \phi + \phi_c$ refers to the accelerated ions, ϕ to the ejected ions (ϕ_h to the 0° ion beam) and ϕ_c to the accelerated confined and/or trapped ions; here, unless otherwise stated, we take $\phi_c \equiv \phi_t \propto \phi$[1] as the quantity of accelerated ions with energy above a convenient low-energy limit $E_0 \gtrsim 50$ keV, say), we consider that a) the spectrum of the trapped/confined ion is the same as that of the ejected ions at 0°, but for an E-independent amplitude factor; and b) an isotropic distribution of ion streams, all with the same spectrum $d\phi_c/dE = 4\pi x d^2\phi_h/dE d\omega$, exists in the region of ion confinement, independently of the type of existing dynamic and thermal conditions in the confinement region (not necessarily close to equilibrium conditions). We can then calculate a neutron yield $Y_{n,c}$ by using a) and b) (i.e., the ejected ion spectrum at 0° of Fig. 2) via

$$Y_{n,c} = n_i \tau \int \sigma(E)\,(2E/m_i)^{1/2}\,(d\phi_c/dE)\,dE$$

with an empirical $n_i\tau \cong 10^{12}$ ($n_i \cong 10^{19}$ cm^{-3}, τ is the ion-confinement time) [5], [11]. This estimated $Y_{n,c}$ is smaller by a factor ~ 50 than the observed Y_n. This leads to the conclusion that $N_i(A) \cong N_i(C) >> N_i(E)$. The confined/trapped spectrum (upper part of Fig. 2) is derived from the observed neutron spectrum by following the method described in the next section. A concentration of the diffuse-plasma current behind the first current sheath in a multiplicity of pinching current sheaths is one of the mechanisms by which an FDE increases the confinement of accelerated ions and Y_n (see Fig. 3 for the results with FDE applications and Section IV) [4].

III. Method of Derivation of the Confined-Ion Spectrum from the Neutron Spectrum

The spectrum of the trapped D^+ ions is obtained from the D–D neutron energy spectrum dY_n/dE_n. dY_n/dE_n is determined from the neutron TOF on a distance $L = 1486$ cm (different values of L and a telescopic normalization of the data have been used [5]) under the assumptions of isotropy of the neutron emission, and no spectrum change from shot to shot; i.e., shots with a different yield Y_n have the same spectrum except for an amplitude factor which is not dependent on the neutron energy E_n. The observed quantity of neutrons $\Delta t_n \Delta E_n d^2Y_n/dt dE_n \cong$ 18–26 with energy between ${}^sE_n = m_n L^2/2(t_s - t_0)^2$ and ${}^sE_n + \Delta E_n$ which generates the leading edge—of duration τ_e—of the neutron signal in one shot[2] determines $d\phi/dE$ via

$$(d^2Y_n/dtdE_n)\,\Delta t_n \Delta E_n = \eta(2/m_i)^{1/2} n_i \int_{t=0}^{\Delta t_n} dt \int_{E(t)}^{E(\Delta t_n - \tau_e)} \cdot \bar{\sigma}(E, 0°)\,(d\phi/dE)\,E^{1/2} dE. \qquad (1)$$

$\Delta t_n \cong$ 10–30 ns is the duration of the neutron emission from hot spots—within the pinch—with density n_i.

The parameter $t \equiv \Delta t + \delta\tau$ that specifies the limits of integration on the right-hand side of (1) is the sum of the delay Δt in the time of emission of neutrons (from the time t_0 of onset of the neutron emission) and of the delay $\delta\tau$ in the neutron time of impact on the detector (from the time $t_s - \tau_e$ of onset of the neutron signal, after correction for the delay of photomultiplier scintillator system: $0 \leqq \Delta t \leqq \Delta t_n$, $0 \leqq \delta\tau \leqq \tau_e$). In terms of the neutron energy E_n we have $t = L(({}^sE_n 2/m_n)^{-1/2} - (E_n 2/m_n)^{-1/2})$, and, by resolving for E_n at the first order in $t/(t_s - t_0)$ we get $E_n(t)$, i.e., $E_n \cong {}^sE_n(1 + 2t/(t_s - t_0))$; ${}^sE_n + \Delta E_n \leqq$

[1] This assumption of proportionality is consistent with the data of Fig. 1(b) only in discharges with Y_n not larger than $2\bar{Y}_n$.

[2] The "leading edge" of the neutron signal from the scintillator detector means here the part of the signal between D–D neutron-signal onset and the point at which the signal amplitude reaches a conveniently chosen value, specifically 1-V on the signal display system (Tektronix 7704). t_s is the time at which the signal amplitude has reached this value; m_n is the neutron mass; neutron emission onset at t_0 = onset time of hard X-ray emission, scintillation detector/photomultiplier systems are used in the saturation mode; typically ${}^sE_n$ = 3.5–4.5 from the data of Fig. 1(a).

$E_n \leqq {}^sE_n$. The energy spread ΔE_n of the neutrons which contribute to the signal from signal onset $t_s - \tau_e$ to saturation time t_s ($\tau_e \cong 10$ ns) depends on Δt_n via $\Delta E_n \cong 2\,{}^sE_n(\Delta t_n + \tau_e)/(t_s - t_0)$ at the first order in $(\Delta t_n + \tau_e)/(t_s - t_0)$. $\bar{\sigma}(E, 0°)$ is a mean value (on the neutron emission cone $\theta = 0° \pm \Delta\theta$ where ${}^sE_n + \Delta E_n \leqq E_n \leqq {}^sE_n$ are satisfied) of the cross section of the D–D fusion reactions with neutron emission close to the direction ($\theta = 0°$) of the accelerated D^+ impinging on the D^+ target. The ion energy $E(t)$ and the interval of integration $\Delta E = E(\Delta t_n + \tau_e) - E(t)$ correlate with E_n, ΔE_n via [14]

$$E_n(E, \theta) = 0.125E\left\{[2(1 + 9.798/E) + \cos^2\theta]^{1/2} + \cos\theta\right\}^2$$

from which $\Delta E \cong 0.9\Delta E_n$ (for $E_n \geq 3.5$ MeV and $\theta = 0°$, where E_n has maximum value). $\tau (\cong \Delta t_n - \tau_e)$ is the D^+ confinement time within the hot spots where a multiplicity of streams (D^+ microbeams which reflect the filamentary structure of the pinch on a micrometer space scale) are accelerated in all directions $d\phi/dE$ can be considered independent on time between t_0 and $t_0 + \tau$ and the product $\bar{\sigma}(E, 0°)\,(d\phi/dE)\,E^{1/2}$ is only weakly dependent on E so that it can be brought out of the integration because of the small value of $\Delta E(-100$ keV) in each shot. η accounts for efficiency of the scintillation detectors, detector-geometry, neutron absorption, etc. (detector efficiency and calibration are the same as reported in [5]).

These approximations simplify (1) into

$$(d^2Y_n/dtdE_n)\,\Delta t_n \Delta E_n = \eta(2/m_i)^{1/2} n_i \bar{\sigma}(E, 0°)\, d\phi/dE\, E^{1/2} \cdot \int_{t=0}^{\Delta t_n} dt\big(E(\Delta t_n + \tau_e) - E(t)\big). \qquad (2)$$

By substituting $E(\Delta t_n + \tau_e) - E(t)$ with $0.9({}^sE_n + \Delta E_n - E_n)$, dt from $dt = L(m_n/2)^{1/2}\, dE_n/2\,{}^sE_n^{3/2}$ and the limits of integration (the upper limit with $E_n(t = \Delta t_n)$, the lower limit with ${}^sE_n$) we get, after carrying out the E_n integration:

$$(d^2Y_n/dtdE_n)\,\Delta t_n \Delta E_n = \eta(2/m_i)^{1/2} n_i \bar{\sigma}(E, 0°)\, d\phi/dE \cdot E^{1/2} 0.9\, L^{-1}(2/m_n)^{1/2}\,{}^sE_n^{3/2}(\Delta t_n^2 + 2\tau_e \Delta t_n).$$

From this expression we obtain $d\phi/dE$ by entering the experimentally determined values of ${}^sE_n$, Δt_n, τ_e, and $\Delta t_n \Delta E_n d^2Y_n/dtdE_n$.

IV. Field Distortion Elements and Y_n

The values of Y_n observed in different series of discharges with FDE (a circular KE) and without FDE under the same conditions (V_0, W_0, and filling pressure) are reported in Fig. 3.

The variations of the pinch structure which correspond to the current-density increase in the current sheath (as it is assessed by magnetic probes in the interelectrode gap) from the early stage of the discharge have also been observed by simultaneously taken pinhole images of the pinch, from particle emission and X-ray emission in the same shot and at the same angle, with a sandwich of X-ray film (on the back side), and of a ~200-μm-thick CR-39 plate (on the front side) [1], [2]. These images show that a tapered part of the pinch appears on the image side far from the electrodes more frequently (in ~70 percent of the shots) in discharges with FDE than in those without FDE. In the latter case the tapered part (~1 mm diameter) of the image is absent in ~80 percent of the discharges and only the diffuse part (with a diameter of $\gtrsim$4 mm) is observed [1], [13]. These data and the data reported in Fig. 1(b) indicate a better confinement of the ions in a smaller region of space up to the time of the pinch explosion if we use a KE as compared to discharges without FDE. The maximum value of Y_n and of the mean value $\bar{Y}_n$ of Y_n over series of ~10^3 discharges increase by a factor $\gtrsim 3$ if suitable FDE's are used.

The variations of Y_n from shot to shot (with or without FDE) are linked to relatively small variations of the main

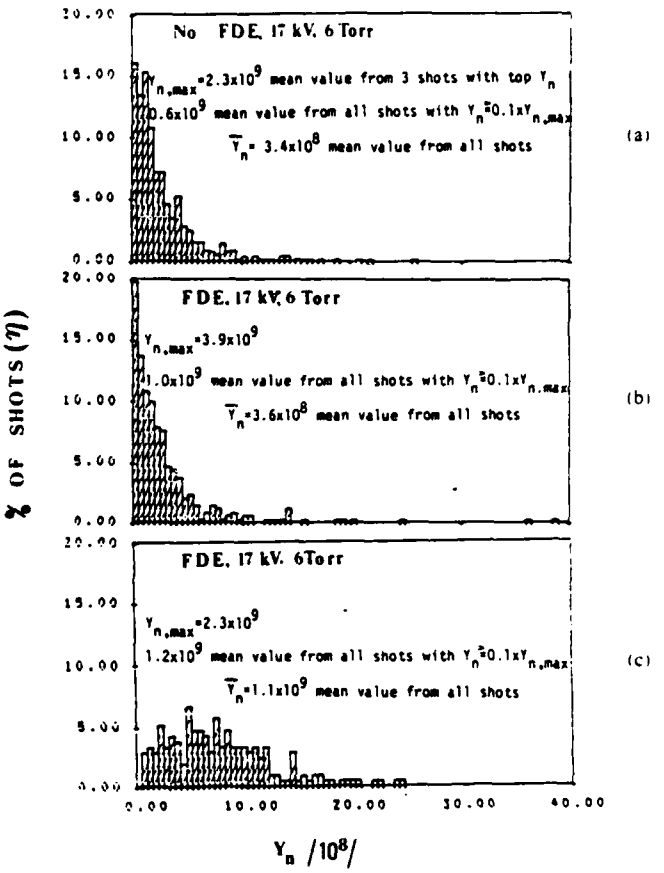

Fig. 3. A field distortion element (circular KE) sharpens the interelectrode current distribution by concentrating it in $\gtrsim$ two sheaths. Percentage η of shots with a neutron yield between Y_n and $Y_n + \Delta Y_n$ ($\Delta Y_n = 5 \times 10^7$) versus Y_n without knife edge (in (a)), with KE of length 7.5 mm in contact with the surface of the insulator (pyrex sleeve) at the breech of the PF (in (b)) and at a distance Δ from the insulator surface (in (c)). Note the elimination of misfirings (i.e., of shots with $Y_n < 5.10^7$) if a suitable spacing Δ between KE and insulator is used as reported in Fig. 4.

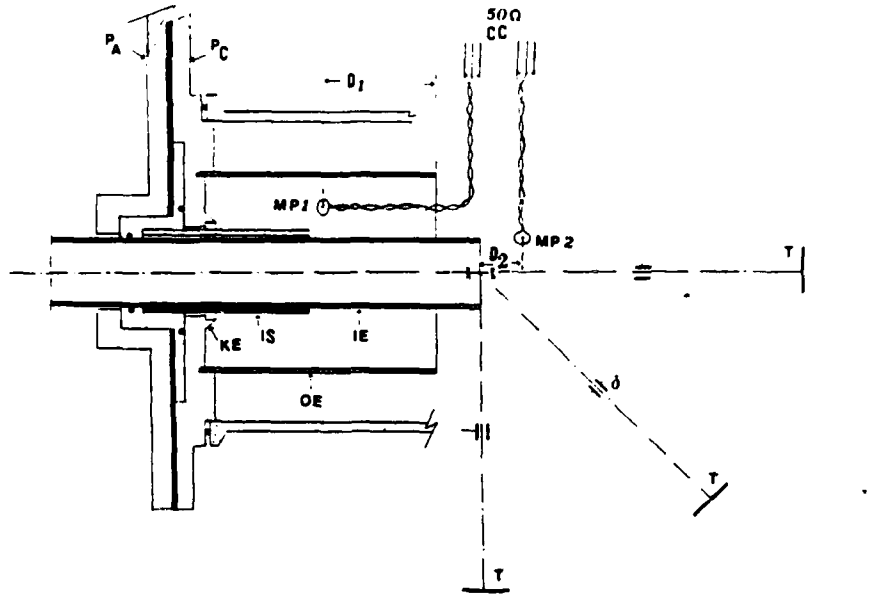

Fig. 4. Cross section of PF electrodes (OE, IE), pyrex insulator sleeve (IS), power-transmission plates (P_A, P_C, breech side), and field-distortion element (KE), with consistent scaling (the external radius of the inner electrode (IE) anode is $r_0 = 36$ mm). Magnetic probes (MP1, MP2) have a 2-mm-diameter loop with center at a radial distance $r = r_0 + 1$ cm and $r = r_0$, respectively (the coated wire with electrostatic shielding is sealed in a 3-mm diameter pyrex pipe and connected to a 50-Ω coaxial cable (CC) with solid copper shielding: ($D_1 = 5$ or 2.5 cm, $D_2 = 1$ cm). The angular distance (azimuthal coordinate) of MP1 from MP2 is 90°. The same details of the current sheath structure (on a ~ 10-ns time scale) appear in each shot in both MP1 and MP2 signals. This confirms a good azimuthal symmetry in the current density j_r in agreement with data from current sheath luminosity [17]. A Rogowski coil between P_A and P_C monitors the variations with time of the electrode current I. Arrangement of three pinhole cameras and CR-39 ion targets (T) is shown (pinhole diameter $\delta = 150$ μm, and MP not in scale). The distance between T and the ion source (xx) is ≅ 15 cm.

(leading) current sheath in the plasma. We have used two magnetic probes (MP1, MP2) for determining in each shot ($V_0 = 15$ kV, $p = 3$–6 torr) the local rate of increase $\partial B_\theta/\partial t$ of the azimuthal magnetic field B_θ, i.e., the radial current density $j_r \cong \partial B_\theta/u\partial t$ (u is the velocity of the current sheath at the probe location) at two different locations in the interelectrode gap (Fig. 4). With an FDE as in Fig. 4—a circular KE near the surface of the insulator sleeve (IS) which has provided so far the best result [15] in terms of Y_n—we find in all shots that j_r in the region between the two probes is lumped in a single current sheath (with an internal structure) of thickness ~ 1 cm up to the first sharp drop of the electrode current I during sheath-inductance surge and pinch disingration. The main current sheath profile presents clear but modest variations of lumpiness from high-Y_n to low-Y_n shots. We can divide the shots of one experimental run with the mean value $\bar{Y}_n$ in different groups depending on Y_n. The group with Y_n in the interval $(2 \pm 0.5) \cdot \bar{Y}_n$ has the main $\partial B_\theta/\partial t$ peak in the MP1 and MP2 signals, higher by 20 (±10) percent than—and with FWHM equal within error limits to—the corresponding quantities of the group with Y_n in the interval $(0.2 \pm 0.1) \cdot \bar{Y}_n$ (at 3 and 6 torr).

The average velocity $\bar{u} = D/t_{1,2}$ ($t_{1,2}$ = time spacing between the $\partial B_\theta/\partial t$ peak from MP1 in the MP2 signal peak; D = MP1 to MP2 distance) has essentially the same value as the mean value of u on the same distance D from a point-by-point determination of u by optical means [16] in the same PF machine without FDE. This justifies, in assessing j_r, the use of typical values $u = 4(\pm 0.2)$ cm/μs for MP1 ($D_1 = 2.5$ cm) and $u = 10(\pm 0.5)$ cm/μs for MP2 at 6 torr consistently with previous measurements [16]. Local distortions of $\partial B_\theta/\partial t$ from the interaction of MP with the sweeping current sheath [17] can hardly affect the main features of the j_r profile.

V. Conclusions

A relatively small fraction (~ 1–2 percent) of the accelerated ions with energy $E \gtrsim 300$ keV is ejected in the 0° beam. The bulk of the accelerated ions in confined in localized regions within the pinch. Field distortion elements in the interelectrode gap can be successfully used for increasing the quality of the current sheath (as it is expressed by the peak values of the current density), the ion confinement, and the neutron yield as an alternative method to the use of plasma-focus operation at high voltage (e.g., ≳ 40 kV). The electric field increase produced

by field distortion elements can be at least as effective as the high-voltage operation [18].

References

[1] V. Nardi, C. M. Luo, and C. Powell, "Anisotropy of the ion energy spectrum from Thomson spectrometers," in *Proc. Plasma Focus/Z-pinches Workshop* (Warsaw, Poland), Sept. 1985, 1985, p. 112.

[2] V. Nardi, C. Powell, W. Prior, and W. H. Bostick, "Ion imaging and energy spectrum from the plasma focus ion emission," in *Proc. 11th Eur. Conf. Controlled Fusion and Plasma Phys.* (Aachen, W. Germany), vol. 7D, Part I, 1983, p. 489.
V. Nardi and C. Powell, "The plasma focus as a source of collimated beams of negative ion clusters and of neutral deuterium atoms," *Am. Inst. Phys. Proc.*, vol. 111, p. 463, 1984.
C. Powell, Ph.D. dissertation, Stevens Inst. of Technology, Hoboken, NJ, May 1985 (University Microfilms, P.O. Box 1346, Ann Arbor, MI 48106).

[3] H. Kilic, Ph.D. dissertation, Stevens Inst. of Technology, Hoboken, NJ, May 1984 (University Microfilms, P.O. Box 1346, Ann Arbor, MI 48106).

[4] V. Nardi *et al.*, "Confinement of MeV ions in a dense pinch," in *Proc. 13th Eur. Conf. Controlled Fusion & Plasma* (Schliersee), 1986, vol. 10-C-1, p. 368.

[5] W. H. Bostick, V. Nardi, and W. Prior: "Observation of 10^8 gauss fields and production of 14-MeV D-T neutrons in a deuterium plasma," *Nucl. Fusion*, Suppl. (IAEA-CN-33/E6-3), vol. 3, p. 109, 1975; also in *Proc. 7th Eur. Conf. Nucl. Fusion* (Lausanne, Switzerland), 1975, vol. 1, p. 62.
W. H. Bostick *et al.*, "Radiation damage (blistering) in Al, Cu, Si by exposure to a plasma focus discharge," *J. Nucl. Mater*, vol. 63, p. 356, 1976.

[6] M. J. Bernstein and G. C. Comisar, "Neutron energy and flux distribution from a crossed-field acceleration model of plasma focus and Z-pinch discharges," *Phys. Fluids*, vol. 15, p. 700, 1972.
J. P. Rager *et al.*, EURATOM-ENEA Ric. Energie-Frascati, Italy, Rep. 80.21/cc (1980), 81.43/cc (1981), 82.22/cc (1982).
J. P. Rager *et al.*, "Experiments on neutron production phase at Frascati IMJ plasma focus," *Nucl. Fusion*, suppl. (IAEA-CN-38/G3), vol. 2, p. 209, 1981.
I. F.Belyaeva, "Energy spectra of accelerated deuterons in a plasma focus," *Nucl. Fusion*, vol. 20, p. 1037, 1980.
J. S. Brzosko, B. V. Robouch, and J. Klobukowska, "A macroscopic study of the neutron, gamma- and X-ray emissivity in the Frascati plasma focus," *Fusion Technology*, vol. 12, p. 71, 1987.

[7] A. Mozer, M. Sadowski, H. Herold, and H. Schmidt, "Experimental studies of fast deuterons, impurity and admixture ions emitted from a plasma focus," *J. Appl. Phys.*, vol. 53, p. 2959, 1982.

[8] W. Stygar, G. Gerdin, F. Venneri, and J. Mandrekas, "Particle beams generated by a 6-12.5 kJ dense plasma focus," *Nucl. Fusion*, vol. 22, p. 1161, 1982.

[9] R. L. Gullickson, W. L. Pickles, D. F. Price, H. L. Sahlin, and T. E. Wainwright, "Ion beam in the plasma focus device," in *2nd Int. Conf. Energy Storage, Compression & Switching*. New York: Plenum, 1978, p. 579.

[10] N. V. Filippov, V. A. Bezbatchenko, I. F. Belyaeva, and T. I. Filippova, "Investigation of energetic ion beams in the plasma focus discharge," in *8th European Conf. Controlled Fusion & Plasma Phys.* (Prague), vol. 1, 1977, p. 63.

[11] W. H. Bostick, V. Nardi, and W. Prior, "Production and confinement of high-density plasmas," *N.Y. Acad. Sci. Annals*, vol. 251, p. 2, 1975.
Ja H. Lee, "Fission and activation of uranium by fusion-plasma neutrons," *Atomkernenergie*, vol. 32, p. 76, 1978.
K. Hubner, J. P. Rager, and K. Steinmetz, "Secondary t-d reactions in the Frascati plasma focus," *Plasmabericht* (Institut fur Angewandte Physik, Univ. Heidelberg), p. 18, May 1981.

[12] J. W. Mather, *Methods of Experimental Physics*, vol. 9, Part B, R. H. Lowberg and H. R. Griem Eds. New York: Academic, 1971, p. 187.
W. H. Bostick, V. Nardi, and W. Prior, "X-ray fine structure of dense plasma in a co-axial accelerator," *J. Plasma Phys.*, vol. 8, p. 7, 1972; also *J. Nucl. Mater.*, vol. 63, p. 695, 1976.

[13] V. Nardi, C. M. Luo, and C. Powell, "Ion clusters from focused MA discharges," in *Proc. 6th Int. Conf. High Power Particle Beams* (Kobe, Japan), C. Yamanaka, Ed., June 1986, p. 447.
V. Nardi, in *Proc. 4th Int. Conf. on MG Magnetic Field Generation* (Santa Fe, NM), M. Fowler, Ed. New York: Plenum, 1986, p. 269.

[14] J. B. Marion and J. L. Fowler, Eds. *Fast Neutron Physics*, Part I. New York: Interscience, 1963, p. 68.

[15] V. Nardi, U.S. Patent Appl. 07 037 753, April 13, 1987.

[16] W. H. Bostick, V. Nardi, L. Grunberger, and W. Prior, "Strong turbulence and shock in a plasma coaxial accelerator," in *Proc. Xth Int. Conf. Phenomena in Ionized Gases*, Parson, vol. 1, 1971, p. 237.

[17] F. T. Gratton and N. Fuentes, "Magnetic field propagation across a weakly conducting layer," *IEEE Trans. Plasma Sci.*, vol. 14, p. 240, June 1986.
N. Fuentes and F. T. Gratton, "On the boil-off time of probe surfaces in plasmas," *IEEE Trans. Plasma Sci.*, vol. PS-14, pp. 575-578, Oct. 1986.

[18] G. Decker, U. Jager, W. Kies, G. Pross, and J. Rybach, "SPEED I: A high impedance high voltage driven fast plasma focus of improved performance," in *Proc. 11th European Conf. Controlled Fusion and Plasma Phys.* (Aachen, W. Germany), S. Methfessel, Ed., European Phys. Soc. Publ., vol. 7-D, (1), Sept. 5-9, 1983, p. 501.

Stimulated Acceleration and Confinement of Deuterons in Focused Discharges—Part II

V. NARDI, L. BILBAO, J. S. BRZOSKO, C. POWELL, D. ZENG, A. BORTOLOTTI, F. MEZZETTI, AND B. V. ROBOUCH

***Abstract*—New methods of increasing, by a factor greater than 5, the neutron yield/shot Y_n from D–D fusion reactions in a plasma focus (PF) enhance both the D^+-ion acceleration to energy values $E_d > 1$–8 MeV and the ion confinement in the pinch region. Nuclear activation of C and N in the (doped) filling gas of the discharge chamber and of solid targets of C and BN bombarded by the ion beam in the direction of the electrode axis (0°) confirms earlier determination of the energy spectrum of the trapped ions ($d\phi_t/dE \propto \phi_{0t}E^{-m}$) and of the ejected beam ($d\phi_b/dE \propto \phi_{0b}E_d^{-m}$, $m = 2.5 \pm 0.5$ for 0.1 MeV $\leq E_d \leq$ 3 MeV). A Thomson (parabola) spectrometer with nanosecond time resolution determines the time of emission $t(E)$ of the beam at 0°. Ion acceleration and trapping occur within the small (filamentary) elements of the magnetic fine structure of the pinch, which can be dispersed on a relatively large confinement volume after the pinch disintegration. We find that $\phi_t/\phi_b \lesssim 10$–$10^3$ for $E_d \geq 1$ MeV, depending on Y_n.**

I. Introduction

INDUCTIVE-FIELD acceleration of ions from the rapid decay of the pinch magnetic field and ion trapping in neighboring high-field regions are enchanced by suitable field-distortion elements (FDE's) inserted in the plasma focus (PF) interelectrode gap (Mather geometry: capacitor bank energy $W \sim$ 6–80 kJ at 16–60 kV) [1]. The FDE concentrates the interelectrode current on a thin current sheath (CS), starting from the onset of the discharge at the breech, and effectively eliminates diffuse distributions of current behind a high-density CS. Another advantage of using an FDE is the virtual elimination of bad shots, i.e., of the shots with $Y_n \leq \bar{Y}_n/20$ ($\bar{Y}_n$ is the mean value of Y_n over thousands of shots in the same condition). The relatively small fluctuations of Y_n from shot to shot with an FDE reflect more the randomness of the processes involved in the pinch disintegration and fine-structure decay than the dispersion of a sizable fraction of the current in a diffuse low-density flow behind the pinching CS. The pinch is formed by a multiplicity of filaments of diameter $\sim$0.5 mm which have been observed in our laboratory (and extensively reported in the literature) by image converter photographs [2], and by schlieren and shadowgraph methods [3], i.e., the same techniques used for the observations of the filamentary structure of the CS at any earlier stage of the discharge. The existence of a fine structure of the plasma-current filaments on an even smaller space scale ($<$0.1 mm) is detectable with other high-resolution methods [4].

One of the mechanisms of particle acceleration in the PF pinch is unambiguously linked to the filaments with the smallest diameter by our observations on filtered images of the pinch from the pinch-particle emission. Pinhole cameras (at 45°, 90°, etc.) with a 150-μm-diameter pinhole form the sharp-profile image of the pinch on a CR-39 plate on which a nonuniform distribution of ion tracks is etched. A grid filter shows that hot spots of ions with $E_d \gtrsim 2$ MeV inside the pinch image have a diameter $\delta \sim 100$ μm, i.e., smaller than the pinhole diameter. This implies a multiplicity of sources of highly collimated beams with transversal linear dimensions $\lesssim 100$ μm. embedded in more diffuse sources of lower energy ions [5].

Ion "confinement" (in an $\sim$2-cm-diameter region which includes the pinch and is determined by the large-scale magnetic field) and ion "trapping" (inside the fine-structure filaments of the pinch and in the pinch fragments, after pinch disintegration) are used here with a somewhat different meaning, as specified in [6]. A quantitative assessment of inductive-field acceleration of ions from the rapid decay of the pinch magnetic field and ion trapping in neighboring high-field regions was carried out in [6] from the following: a) the determination of the confined ion spectrum via the observation of the neutron spectrum for neutron energy values $E_n \cong$ 3–5 MeV; b) the ejected ion spectrum (via magnetic analyzers, spectrometers, differential filters, and Faraday collectors) on a fraction ($E_d \lesssim 3$ MeV) of the total energy interval 0.1 keV $\lesssim E_d \lesssim$ 8 MeV on which the spectrum was determined [7]; and c) filtered imaging of the pinch by particle emission in different directions. The limitations on E_d imposed in [6] by the low emission intensity of neutrons with energy above $E_n \cong 5$ MeV is bypassed here by using nuclear activation of gaseous and solid targets.

II. Nuclear Activation of C, N, and B

The filling gas (D_2) of the discharge chamber was doped with CH_4 or with N_2 up to an atomic fraction $\eta =$

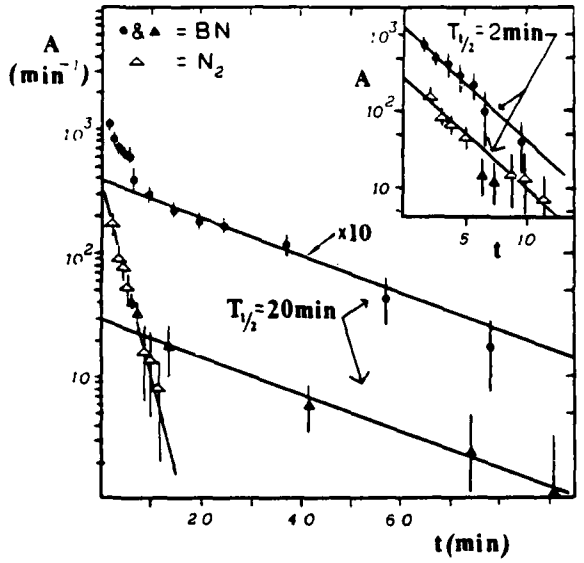

Fig. 1. β^+ activity A versus $\bar{t}$ (time of activity observation) from shot #1273 (upper line, $Y_n = 1.2 \cdot 10^9$) with solid BN target and pure D_2 filling, and from shot #1339 (lower line, $Y_n = 6.8 \cdot 10^8$) with BN target and N_2 doping (7 percent by pressure $\eta = 0.07$) of D_2 filling at a total pressure $p = 6.5$ torr ($W_0 = 7$ kJ at 17 kV). The reported values of A lack the necessary normalization for different geometric factors involved in the activity measurements on the gas (volume) and on the solid target. The data points • and ▲ refer to the activity of the solid target, the symbol △ refers to the gas (volumetric) activity. The beam-induced activity from $^{10}B(d, n)^{11}C(\beta^+)$ is reported for both shots. In the upper right corner, the activity of ^{15}O from gas and solid target of shot #1339 (lower line) and solid target of shot #1273 ($\times 10$) are reported with an expanded time axis. Refilling the discharge chamber after each shot (max $Y_n = 2.7 \cdot 10^9$, $\bar{Y}_n = 6 \cdot 10^8$ with doping; max $Y_n = 3.8 \cdot 10^9$, $\bar{Y}_n = 1.1 \cdot 10^9$ with pure D_2). Period of PF circuit 9.5 μs, discharge chamber ϕ_i diameter 15.3 cm, length $h = 30$ cm; center electrode ϕ_0 diameter 3.4 cm, $h = 13.8$ cm; insulator ϕ_0 diameter 4.5 cm, $h = 5.2$ cm; outer electrode ϕ_i diameter 9.9 cm, $h = 11.8$ cm; distance Geiger counter window/exposed target surface 3 cm. C_3D_8, instead of CH_4, was used in many series of shots for gas C target activation, with the same results. The error bar is the statistical error.

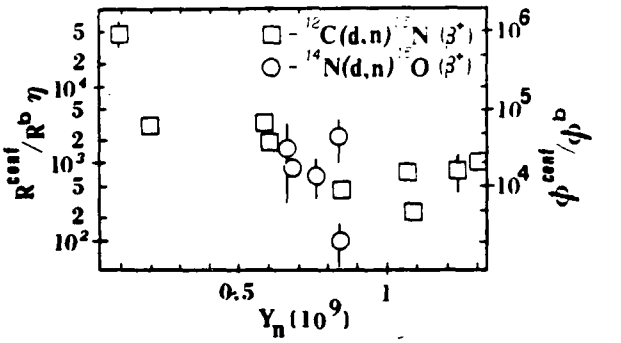

Fig. 2. Ratio of the quantity R_{conf} of radionuclei (^{13}N, β^+ 1.3 MeV or ^{15}O, β^+ 1.72 MeV) generated in the gas by confined D^+ ions and of the quantity R_b of radionuclei of the same species generated in the solid target by the D^+ beam at 0°, as a function of Y_n in the same shot. $R = A/\epsilon\lambda\Omega$, where $\epsilon = 0.8$ accounts for the efficiency of the Geiger counter; λ ($T_{1/2}$ = half-lifetime) is the decay constant of the radionuclei; the fraction Ω of detected β^+ is controlled by detector/activity source geometry ($\Omega = 3.2 \times 10^{-3}$ for the gas-volume-activity, $\Omega = 0.118$ for the solid target). The corresponding values of $\phi_{conf}/\phi_b = \gamma R_{conf}/\eta R_b$ are indicated on the left vertical axis for a thin-plasma target. $\gamma = 0.2$ is a conversion factor that weakly depends on the D^+ confinement time τ ($n\tau \simeq 3 \cdot 10^{11}$, with $n \simeq 10^{19}$ cm^{-3} from pinch density and $\tau = \tau_n$, $\tau_n = 30$ ns is the shortest duration of the PF neutron pulse with scintillation detector at 10 cm from the source), on τ_{rel}, the D^+-energy relaxion time in the pinched plasma and on the D^+ spectra (for a thin-plasma target $\gamma = S/G$; $S = \int Y(E)E^{-m}a(E)dE$, $G = \eta_d \Delta x \int E^{-m}\sigma(C + d)dE$; the limits of integration are 0.3–10 MeV; $Y(E)$ is a thick-target reaction yield (defined as in [11]), $a(E)$ is the β^+ absorbtion of the solid target, $\sigma(C + d)$ is the cross section for reaction induced by D^+ in ^{12}C target.

2–7 percent of C or N. The volumetric activity from $^{12}C(d, n)^{13}N(\beta^+)$ or from $^{14}N(d, n^{15}O(\beta^+)$ was measured after each shot with an external Geiger counter through a 3-cm-diameter window sealed with a 50-μm-thick capton foil. In the same shot, a solid target (3-cm-diameter) of C or of boron nitrate (BN) with ~20 percent of ^{10}B was located, at 0°, at a distance of 18 cm from the end of the PF center electrode (anode). The β^+-activity from the solid target was measured for each shot by alternatively exposing to the Geiger view the bombarded side of the solid target and the discharge chamber with the activated gas. The results are presented in Figs. 1 and 2. In our estimate, the D^+ spectrum amplitudes ϕ_{0t}, ϕ_{0b} can be considered as not dependent on E_d for $E_d \gtrsim 0.05$ MeV in agreement with [6]–[9] and, because of the sharp localization in time and space of the neutron source in our experiments [10], we take $\phi_t \simeq \langle \phi_t \rangle = \phi_{conf}$, where $\langle \phi \rangle$ means an average on volume and duration τ_n ($=$ confinement time τ) of the neutron source. The simultaneous use of gaseous and solid targets in the same shot characterizes the difference of method and objective (specifically, the estimate of ϕ_t/ϕ_b) of this work from those of an earlier pioneering work [9] on the nuclear activation of solid targets for determining energy and angular distribution of the PF D^+ emission. Two different lines of thought, based on a) $\tau \sim \tau_{rel}$ ($0.1 < \tau_{rel}/\tau < 5$, τ_{rel} = D^+ energy relaxation in the pinched plasma)—typical of a thick plasma target—or b) $\tau << \tau_{rel}$—typical of a thin plasma target—can be followed in estimating ϕ_t/ϕ_b from R_{conf}/R_b, with $m = 2.5$, $\gamma \simeq 0.2$ for a) and $\gamma \simeq 20$ for b), as in Fig. 2. A good agreement between $\phi_{0,conf}(R)$—from nuclear activation data—and $\phi_{0,conf}(Y_n)$—from Y_n (see [6])—is obtained with b) and a particle density $n = 10^{21}$ cm^{-3} with a τ ($\simeq 0.3$ ns) fitting a thin-plasma target. Alternatively, with the thick-plasma target we find $\phi_{0,conf}(Y_n) \simeq 10^{-2} \cdot \phi_{0,conf}(R)$. This provides a good reason for preferring b) over a). We can easily reconcile b) with a $\tau_n >> \tau$ if the bulk of the neutron source is conceived as a collection of a larger number of very small (thin, dense) sources (each with typical linear dimensions $\Delta x \simeq 100$ μm) in the pinch region (appropriately in this case, τ should be considered as a transit time through Δx).

III. Other Measurements and Conclusions

The FDE effect on Y_n (and by inference, on B, C, N nuclear reactions) is shown in Fig. 3, for shots at 3 torr. At this pressure, $\bar{Y}_n$ increases by a factor of 2, at 6 torr, by a factor >3, as compared with shots without FDE [6] (the increase of $\bar{Y}_n$ is >5 if we also enter in the estimate of $\bar{Y}_n$ the shots with a very low Y_n, i.e., $3Y_b < Y_n < 5 \times 10^7$, which are frequently observed without FDE; Y_b is the background count). The relative variation in the current distribution is correspondently small [6], of the order

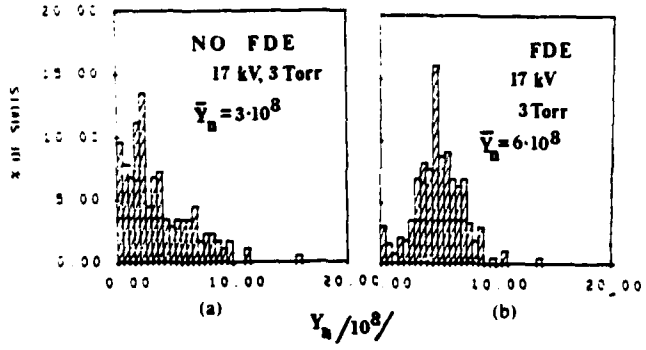

Fig. 3. Histogram with percent of shots with a neutron yield between Y_n and $Y_n + \Delta Y_n$ ($\Delta Y_n = 5 \times 10^7$) as a function of Y_n (a) without FDE, and (b) with FDE. Note change of distribution shape from (a) to (b). See [1].

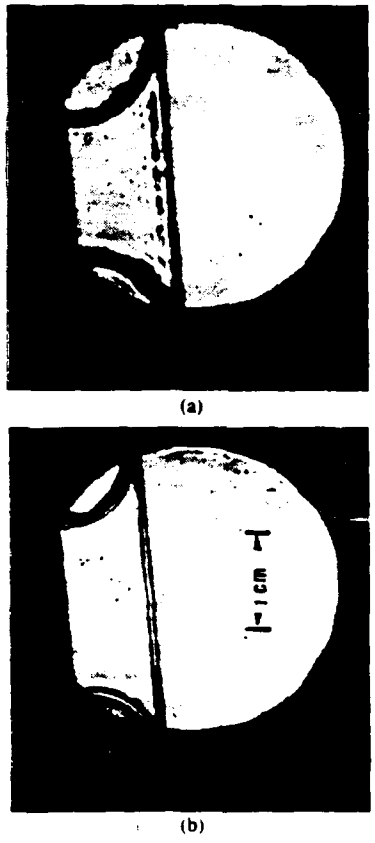

Fig. 4. Typical schlieren image of the imploding current sheath at the time $t_0 = 90 (\pm 10)$ ns at which the CS sweeps a magnetic probe (*MP*2 of [6]) located 1 cm off the front end of the center electrode/anode (the flat profile at the left is the anode front end): (a) shot without FDE ($Y_n \cong \bar{Y}_n$); (b) shot with FDE (a circular knife edge at the "breech," as in [6, Fig. 4], $Y_n \cong \bar{Y}_n$). The current filaments (fine structure) of the CS [2], [3] have a diameter (≤ 0.5 mm), somewhat greater in (a) than in (b). This is the cause of the wiggled pattern (right side of the image in (a)) in the current sheath.

of 10 percent, but evidently has a critical role, as we can assess from Y_n and from the variation of the pinhole image of the pinch via particle emission on CR-39 targets (image morphology and energy spectrum of the image-forming ions [5]).

The current-sheath thickness at $t = t_0 - \Delta t$ ($\Delta t = 50$–100 ns) from magnetic probes and schlieren with a nanosecond (UV N_2) laser pulse is, within the error bar, the same with or without FDE (see Fig. 4); at 6 torr, however, fluctuations wider by a factor $\simeq 2$ are observed without FDE. Thomson spectrometers with nanosecond time resolution (see [1] and Fig. 5) show that D^- with $E_d =$

(a)

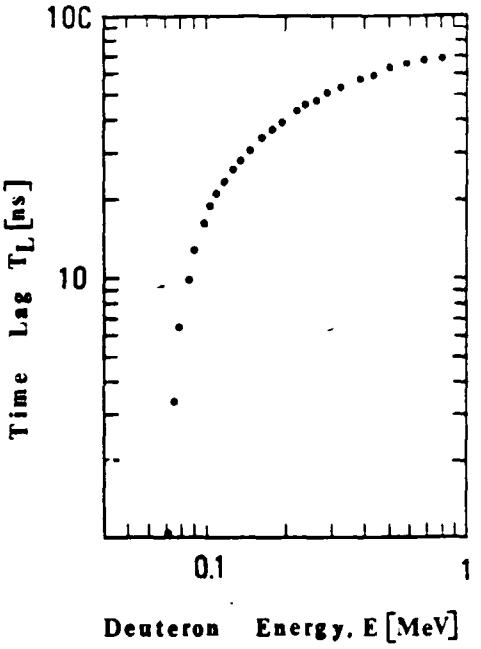

(b)

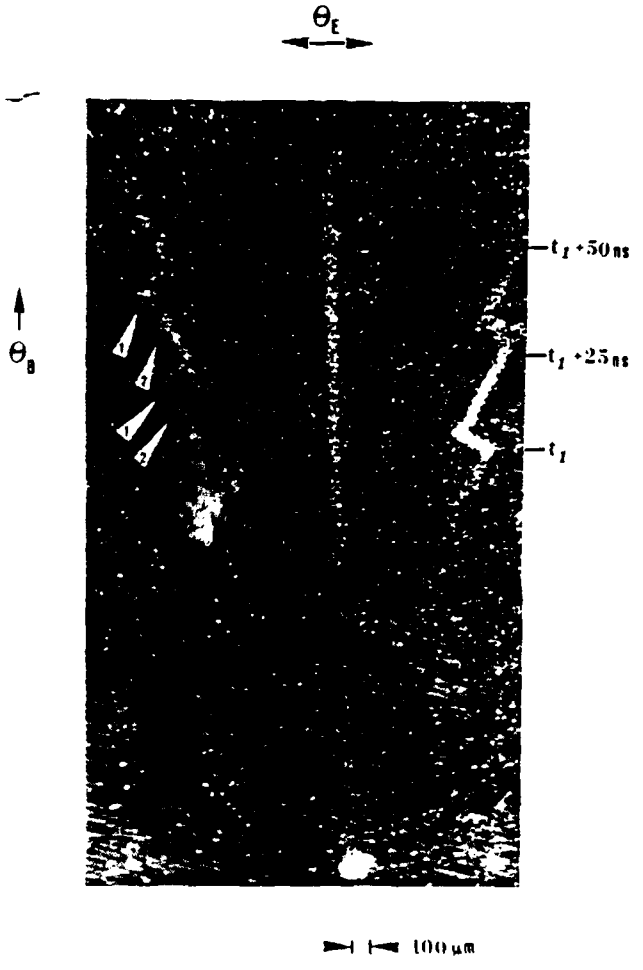

(c)

Fig. 5. Patterns of etched ion tracks on CR-39 targets of a compact Thomson (parabola) spectrometer: each target is exposed to a single shot. (a) A periodic electric field $\vec{E}$ (period T_0 = 17 ns, 1.5 kV) is applied to the pole pieces of diameter 2.5 cm with B = 5 kG and spacing d = 4.5 mm between poles. Note that three distinct beam components produce the pattern in (a). The time shift between two components is determined except for multiples of T_0. The continuous variations of a periodic E are convenient for determining the variation of $E(t)$ of each component of the beam, at the beam source, as a function of relative time (time lag) T_L from the time of emission of D^+ with, e.g., E = 70 keV. The method and the result were reported in [1]. D^+ with E_0 = 1 MeV are ejected about 100 ns later than 70 keV D^+ (T_L = 100 ns) as reported in (b). (c) Pattern (segmented parabolas) obtained with a stepped (ramped) $\vec{E}$ = $\vec{E}_0$ + $\vec{E}_1(t)$ on the pole pieces. E_{0z} = 4 kV; $E_1(t \leq t_1)$ = 1 kV decreases after t_1, in a 5-ns interval, at each step of 33 percent of the value in the previous step (spacing between steps is 25 ns). The left-hand side of (c) (shot #531) has a two-component beam impacting at the same time t_1 for E_{z1} = 175 keV, E_{z2} = 150 keV (difference in time of emission ΔT_L = 10 ns) and at t_1 + 25 ns for E_{z1} ≲ 100 keV (t_1 = t_0 + 170 ns; t_0 = time of dI/dt peak in the electrode current signal I).

E_{d0} = 200 keV are ejected at 0° at $t = t_0$ (= time of peak of the electrode-current signal $|dI/dt|$) and earlier if $E_d < E_{d0}$ or later if $E_d > E_{d0}$. A thin, rather than a thick, plasma target fits both R and Y_n groups of data well.

REFERENCES

[1] V. Nardi *et al.*, "Confinement of MeV ions in a dense pinch," in *Proc. 13th European Conf. Controlled Fusion and Plasma*, vol. 10-C-1 (Schliersee), 1986, p. 368.

[2] W. H. Bostick, L. Grunberger, and W. Prior," Vorticity and neutrons in the plasma focus," in *Proc. 5th Symp. Thermophysical Properties*, 1970, p. 495.

[3] W. H. Bostick, V. Nardi, and W. Prior, in *Dynamics of Ionized Gases*, M. J. Lighthill *et al.*, Eds. Tokyo, Japan: Tokyo Univ. Press, 1971, p. 375.

[4] V. Nardi, W. H. Bostick, J. Feugeas, and W. Prior, "Internal structure of electron-beam filaments," *Phys. Rev.*, vol. 22A, p. 2211, 1980.
Proc. 2nd Conf. Energy Storage, Compression and Switching, vol. 2. New York: Plenum, 1978, p. 449.

[5] V. Nardi, C. M. Luo, and C. Powell, "Ion clusters from focused MA discharges," in *Proc. 6th Conf. High-Power Particle Beams* (Kobe, Japan), 1986, p. 447.
Proc. 4th Conf. Megagauss Magnetic Field Generators (Santa Fe, NM), 1986, p. 269.

[6] V. Nardi *et al.*, "Stimulated acceleration and confinement of deuterons in focused discharges, Part I," *IEEE Trans. Plasma Sci.*, this issue, pp. 000–000.

[7] V. Nardi and C. Powell, "The plasma focus as a source of collimated beams of negative ion clusters and of neutral deuterium atoms," *Amer. Inst. Phys. Proc.*, vol. 111, p. 463, 1983.

[8] R. L. Gullickson, W. L. Pickles, D. F. Price, H. L. Sahlin, and T. E. Wainwright, "Ion beam in the plasma focus device," in *Proc. 2nd Conf. Energy Storage, Compression and Switching*, vol. 2. New York: Plenum, 1978, p. 579.

[9] R. L. Gullickson and H. L. Sahlin, "Measurements of high energy deuterons in the plasma focus device," *J. Appl. Phys.*, vol. 49, p. 109, 1978.

[10] W. H. Bostick, V. Nardi, and W. Prior, "Space-time structure of neutron and X-ray sources in a plasma focus," *Nucl. Fusion Suppl.*, vol. 3, p. 497, 1977; see also, *Proc. 2nd Conf. Energy Storage, Compression and Switching*, vol. 2. New York: Plenum, 1978, p. 267.

[11] J. S. Brzosko, H. Conrads, J. P. Rager, B. V. Robouch, and K. Steinmetz, "Investigation of high-energy deuterons in a dense plasma focus device by means of neutrons emitted in the Li + D process," *Nucl. Techn./Fusion*, vol. 5, p. 209, 1984.